5-30-2008

Finding Concealed Active Faults: Extending the Southern Whidbey Island Fault across the Puget Lowland, Washington

Brian L. Sherrod
University of Washington - Seattle Campus

Richard J. Blakely
U.S. Geological Survey

Craig S. Weaver
University of Washington - Seattle Campus

Harvey M. Kelsey
Humboldt State University

Elizabeth Barnett
Humboldt State University

See next page for additional authors

 DOI: 10.1029/2007JB005060

JOURNAL OF GEOPHYSICAL RESEARCH, VOL. 113, B05313, doi:10.1029/2007JB005060, 2008

Finding concealed active faults: Extending the southern Whidbey Island fault across the Puget Lowland, Washington

Brian L. Sherrod,[1] Richard J. Blakely,[2] Craig S. Weaver,[1] Harvey M. Kelsey,[3] Elizabeth Barnett,[3] Lee Liberty,[4] Karen L. Meagher,[1] and Kristin Pape[4]

Received 20 March 2007; revised 27 November 2007; accepted 18 January 2008; published 30 May 2008.

[1] The southern Whidbey Island fault zone (SWIF), as previously mapped using borehole data, potential field anomalies, and marine seismic reflection surveys, consists of three subparallel, northwest trending strands extending ~100 km from near Vancouver Island to the northern Puget Lowland. East of Puget Sound, the SWIF makes landfall between the cities of Seattle and Everett but is concealed beneath a thick mantle of young glacial deposits and vegetation. A ~20-km-wide, northwest trending swath of subparallel, low-amplitude aeromagnetic anomalies crosses this region of the Puget Lowland and is on strike with the SWIF. The most prominent aeromagnetic anomaly, the Cottage Lake lineament, extends at least 18 km and lies approximately on strike with the SWIF on Whidbey Island. Subtle scarps and topographic lineaments on Pleistocene surfaces, visible on high-resolution lidar topography at a number of locations along the SWIF, lie on or near these magnetic anomalies. In the field, scarps exhibit northeast-side-up and vertical relief of 1 to 5 m. Excavations across several lidar scarps lying on or near magnetic anomalies show evidence for multiple folding and faulting events since deglaciation, most likely above buried reverse/oblique faults. Excavations in areas away from magnetic anomalies do not show evidence of tectonic deformation. In total, paleoseismological evidence suggests that the SWIF produced at least four earthquakes since deglaciation about 16,400 years ago, the most recent less than 2700 years ago.

Citation: Sherrod, B. L., R. J. Blakely, C. S. Weaver, H. M. Kelsey, E. Barnett, L. Liberty, K. L. Meagher, and K. Pape (2008), Finding concealed active faults: Extending the southern Whidbey Island fault across the Puget Lowland, Washington, *J. Geophys. Res.*, *113*, B05313, doi:10.1029/2007JB005060.

1. Introduction

[2] Geologists used to despair in their attempts to find active faults in the Puget Lowland, a region of relatively low strain rates where bedrock geology is obscured by young glacial deposits, thick vegetation, and urbanization. Broad fault zones defined by gravity and seismic reflection surveys helped to focus geologic studies in certain areas, but, even with these tools, geologists were hampered by the lack of exposure. Here we show that high-resolution aeromagnetic surveys, lidar mapping, and field geology allow identification of active faults in regions where bedrock geology is obscured.

[3] Active faults in the Puget Lowland owe their existence in part to oblique subduction of the Juan de Fuca plate beneath North America, and in part to northward migration of the North American fore arc (Figure 1). Geodetic studies using a densified Global Positioning System (GPS) network show that discrete tectonic blocks in the fore arc move northward at a rate of 7–9 mm/y relative to Coastal Mountains of British Columbia [*Wells et al.*, 1998; *Wells and Simpson*, 2001; *McCaffrey et al.*, 2000], with reverse faults and folds at shallow depth in the North American plate accommodating the resulting strain. Several millimeters per year of this displacement are accommodated in the northern Puget Lowland, as shown by the GPS signal remaining after removal of the effects of elastic strain accumulation on the Cascadia subduction zone [*Mazzotti et al.*, 2002]. Occasionally, the accumulated strain is released as large, shallow earthquakes, such as the series of events on several faults in the Puget Lowland about 1100 years ago [*Bucknam et al.*, 1992; *Atwater and Moore*, 1992; *Nelson et al.*, 2003b; *Sherrod*, 2001; *Sherrod et al.*, 2004; *Karlin and Abella*, 1996; *Johnson et al.*, 2004].

[4] In this paper, we describe a program of aeromagnetic mapping, seismic reflection surveys, lidar mapping, and field studies designed to identify active faults, particularly where faults are concealed beneath young sediments, vegetation, or urbanization. Our program begins by identifying aeromagnetic anomalies, including subtle anomalies originating from Pleistocene glacial deposits, to reveal locations

[1] U.S. Geological Survey at Department of Earth and Space Sciences, University of Washington, Seattle, Washington, USA.
[2] U.S. Geological Survey, Menlo Park, California, USA.
[3] Department of Geology, Humboldt State University, Arcata, California, USA.
[4] CGISS/Boise State University, Boise, Idaho, USA.

0148-0227/08/2007JB005060$09.00

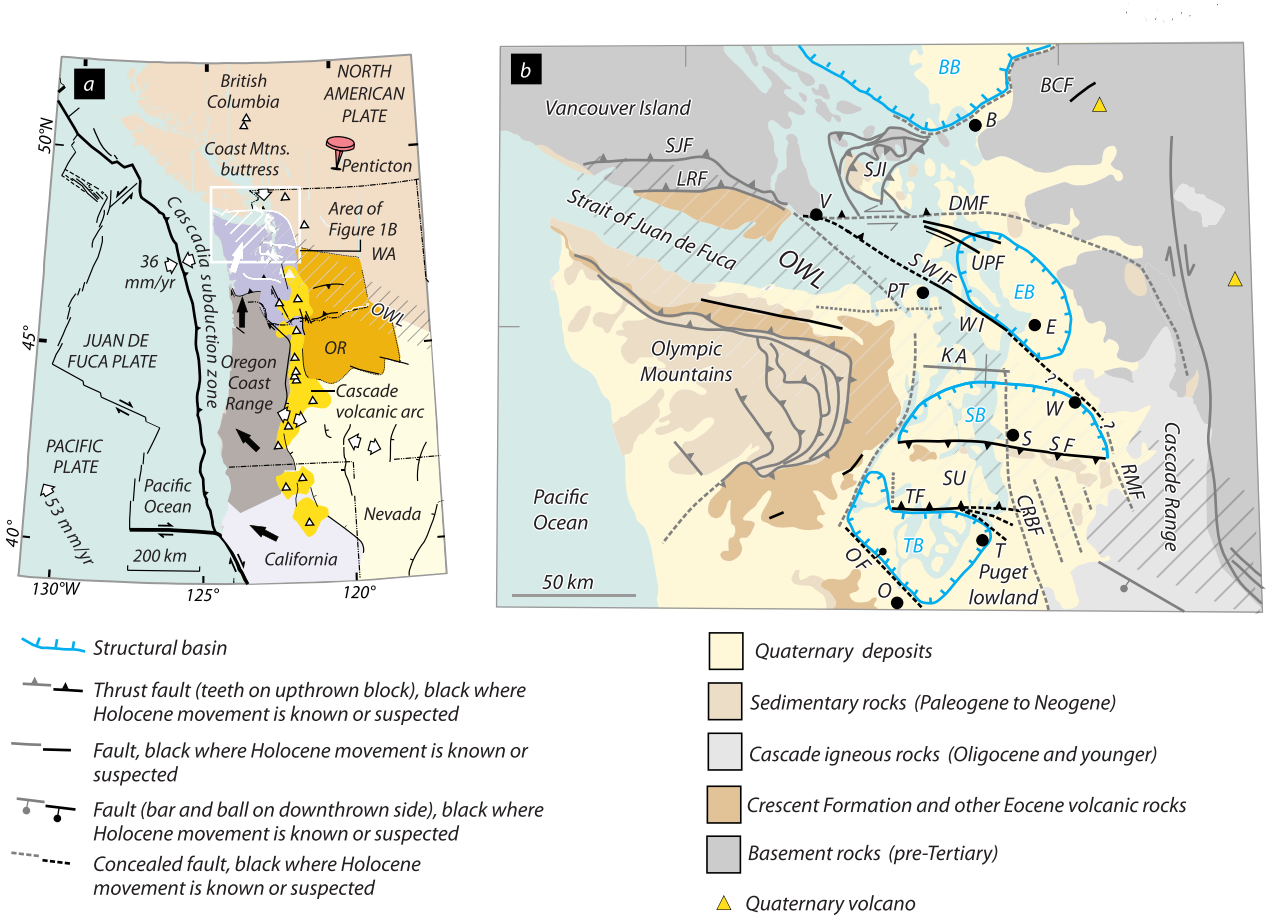

Figure 1. (a) Kinematic model of Cascadia fore arc, simplified from *Wells et al.* [1998] and *Wells and Simpson* [2001]. Northward migration of the Oregon Coast Range squeezes western Washington against North America, producing faults and earthquakes in the Puget Lowland. (b) Generalized map of the Puget Lowland and surrounding regions. BB, Bellingham basin; EB, Everett basin; KA, Kingston arch; SB, Seattle basin; SU, Seattle uplift; TB, Tacoma basin; BCF, Boulder Creek fault; CRBF, Coast Range boundary fault; DMF, Devils Mountain fault; LRF, Leech River fault; OF, Olympia fault; RMF, Rattlesnake Mountain fault; SJF, San Juan fault; SWIF, southern Whidbey Island fault; SF, Seattle fault; TF, Tacoma fault; UPF, Utsalady Point fault; B, Bellingham; E, Everett; O, Olympia; PT, Port Townsend; S, Seattle; T, Tacoma; V, Victoria; W, Woodinville; SJI, San Juan Islands; WI, Whidbey Island. Redrawn from *Brocher et al.* [2001]. Hachured area on both maps shows the general location of the Olympic-Wallowa lineament (OWL) [*Raisz*, 1945].

of possible fault traces (Figure 2). Scarps identified with lidar mapping that fall along or near aeromagnetic anomalies are reconnoitered as candidates for detailed geologic field studies. Where possible, seismic surveys help identify strands with the highest potential for having had young deformation. Finally, the most promising scarps are excavated and logged in an effort to understand the nature and history of deformation.

[5] This paper describes an application of our methodology to the southern Whidbey Island fault (SWIF), specifically where it passes through heavily populated regions between Seattle and Everett, Washington. Evidence provided by airborne and ground magnetic surveys, lidar-based topography, seismic reflection imaging, trench excavations, geologic field studies, and historic midcrustal earthquakes indicates a broad (20 km) zone of tectonic deformation, which we argue is the active SWIF in this urban area.

2. Regional Setting

[6] The southern Whidbey Island fault (SWIF) was originally mapped by *Gower et al.* [1985] on the basis of gravity and magnetic anomalies as a mostly concealed fault extending northwestward from Woodinville to near Port Townsend, a distance of about 50 km (Figure 1). The fault lies within a broad zone bounded by outcrops up to 35 km apart which defines a boundary between pre-Tertiary crystalline rocks and Tertiary Coast Range basalts [*Johnson et al.*, 1996]. This crustal boundary is blanketed by a thick sequence of Quaternary glacial and interglacial sediments. The last glacial advance into the Puget Lowland, regionally

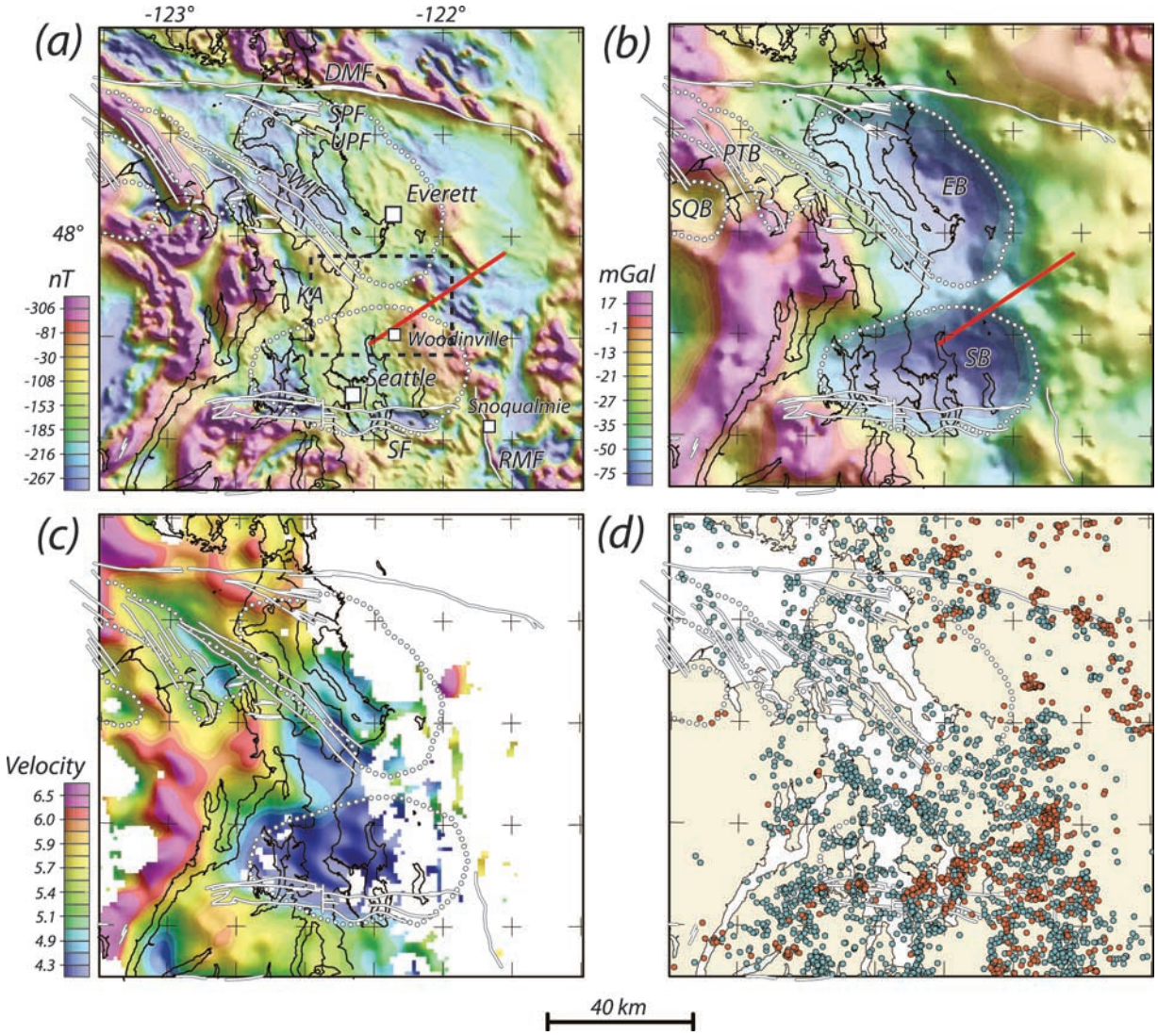

Figure 2. Geophysical framework of the greater Puget Sound region, Washington. (a) Aeromagnetic anomalies [*Blakely et al.*, 1999]. White lines are faults from the U.S. Geological Survey Quaternary fault database (http://earthquake.usgs.gov/regional/qfaults). Black dashed rectangle shows area of Figure 4. DMF, Devils Mountain fault; KA, Kingston arch; RMF, Rattlesnake Mountain fault; SF, Seattle fault; SPF, Strawberry Point fault; UPF, Utsalady Point fault. (b) Isostatic residual gravity anomalies. White dotted lines are deep sedimentary basins manifested in gravity and tomography data. EB, Everett basin; PTB, Port Townsend basin; SF, Seattle basin; SQB, Sequim basin. (c) Seismic velocity at 4 km depth, taken from three-dimensional tomographic model of *Brocher et al.* [2001]. (d) All earthquakes greater than magnitude 1.5 occurring from 1969 to 2006 with RMS <0.25 s and vertical error <1.0 km. Blue dots are earthquakes with depths between 35 and 12 km; orange dots are earthquakes with depths <12 km. Data are from the University of Washington catalog.

called Vashon, culminated around 16,400 cal years B.P. when the glacier disintegrated rapidly, depositing outwash deposits and glacial diamicts [*Porter and Swanson*, 1998]. The Vashon glacier left behind a distinctive fluted topography oriented in the direction of ice flow. In our study area, these flutes are oriented 162° to 175°.

[7] The SWIF lies adjacent to the Everett basin, a structural depression estimated to be 8.5 km deep at its deepest point [*Johnson et al.*, 1996], filled with Tertiary and younger sedimentary rocks, and producing a pronounced negative gravity anomaly immediately northeast of the SWIF (Figure 2b). *Gower et al.* [1985] viewed the SWIF as a single, steeply dipping, north-side-down fault [e.g., *Gower et al.*, 1985; *Yount and Gower*, 1991], presumably on the basis of its spatial association with the Everett basin. More recently, *Johnson et al.* [1996] used seismic reflection profiles on Whidbey Island and in Puget Sound, sea cliff exposures on Whidbey Island, and sparse borehole data to map and interpret the SWIF as a broad fault zone (6 to 11 km wide) dipping steeply to the northeast. They suggested that the SWIF developed in the early Eocene as an arc-parallel strike-slip fault and, responding to oblique convergence of the subducting plate and clockwise rotation of the fore arc, has evolved into a complex transpressional

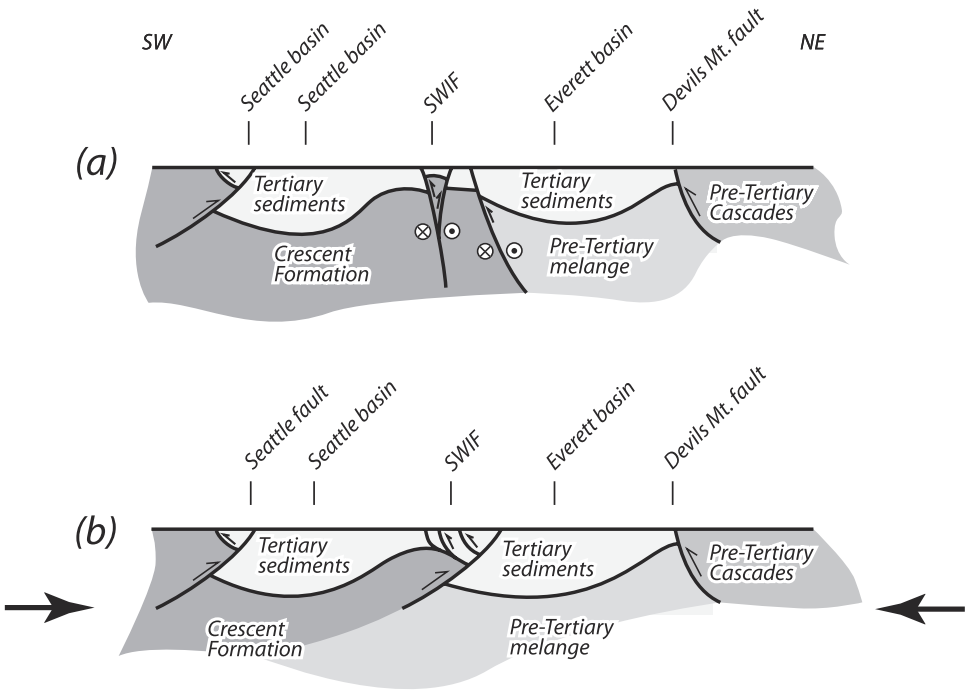

Figure 3. Two conceptual models for the SWIF. (a) The SWIF as an oblique, right-lateral strike-slip fault, sometimes forming transpressional flower structures [*Johnson et al.*, 1996]. (b) The SWIF as an advancing wedge bounded by roof and floor thrusts [*Brocher et al.*, 2005]. In this latter view, surface manifestations of the SWIF are back thrusts that root into a larger roof thrust.

structure exhibiting dextral strike-slip, reverse, and thrust components of displacement. *Johnson et al.* [1996] noted significant structural variability along the SWIF and mapped it as a zone of two to three parallel splays, each with oblique displacement but together exhibiting dominantly right-lateral strike-slip and north-side-up reverse fault displacement (Figure 3a).

[8] *Johnson et al.* [1996] mapped the SWIF northwestward to the eastern Strait of Juan de Fuca. Farther to the northwest, the SWIF passes along the northeastern margin of the Port Townsend basin, identified with seismic tomography [*Brocher et al.*, 2005; *Ramachandran et al.*, 2005], and merges with the Devils Mountain fault near the city of Victoria on Vancouver Island, British Columbia (Figure 2c). We propose in this paper that the southeastward extension of the SWIF crosses the northeastern margin of the Seattle basin (Figure 2) and merges with the Seattle fault and other active structures. If correct, the SWIF extends a minimum of 150 km, from near Victoria to east of Seattle. *Johnson et al.* [1996] found various lines of evidence that the SWIF has been active in Quaternary time, and *Kelsey et al.* [2004] showed evidence from two marshes on opposite sides of the northern strand on Whidbey Island for north-side-up displacement about 3000 years ago, probably associated with a M7 earthquake.

[9] Recent geologic and geophysical studies of the mainland extension of the SWIF [*Blakely et al.*, 2004; *Sherrod et al.*, 2005a] identified a broad (~20 km), northwest striking zone of deformation in the Woodinville area, where individual faults exhibit north-side-up displacement. This sense of displacement seems at odds with the Everett basin immediately northeast of the SWIF, which suggests a long-term history of north-side-down deformation. Using seismic tomographic inversions and other geophysical data, *Brocher et al.* [2005] explained the observed sense of displacement in terms of a roof/floor thrust fault model (Figure 3b), similar to one proposed earlier for the Seattle fault [*Brocher et al.*, 2004]. In their view, the surface expression of the SWIF is produced by northeast dipping back thrusts above a northeastward advancing triangle zone, or wedge, developed in the Eocene Crescent Formation (Figure 3b). Advance of the wedge is accommodated by a master floor thrust on the base of the wedge that dips at shallow angle to the southwest. A roof thrust dips gently northeastward, shoals into the master thrust, and provides a detachment surface for ancillary back thrusts above the advancing wedge. It is important to note that both the model proposed by *Johnson et al.* [1996] and the model proposed by *Brocher et al.* [2005] describe the SWIF as a major crustal boundary separating Tertiary Crescent Formation to the southwest from pre-Tertiary rocks to the northeast.

[10] A number of important questions remain regarding the tectonic evolution and modern day configuration of the SWIF. The SWIF has extreme along-strike variability in structural style, perhaps best reflected by its spatial association with three major crustal depressions: the Port Townsend, Everett, and Seattle basins. The relatively straight SWIF straddles these three basins, with the basins alternating on opposite sides of the fault, and it seems unlikely that the entire SWIF can be assigned to a single tectonic model. The kinematic links with other structures at both the northwestern and southeastern ends of the SWIF also remain unresolved. If continued on strike to the southeast, for example, the SWIF potentially merges with the Seattle

fault [*Pratt et al.*, 1997; *Johnson et al.*, 1994; *Blakely et al.*, 2002], the Rattlesnake Ridge fault [*Walsh*, 1984], the Olympic-Wallowa lineament [*Raisz*, 1945; *Reidel and Campbell*, 1989], and other active structures east of Seattle. How strain is transferred among these crustal structures remains an important unresolved question.

[11] Crustal earthquakes form a complex distribution across the Puget Sound basin (Figure 2d), but several patterns are apparent. Whereas the Seattle basin is seismically active, especially around its margins, the Everett basin is relatively aseismic. In particular, a 400 km^2 region north of Everett is unique in the Puget Lowland in having no shallow earthquakes larger than M 1.5 since 1969. Essentially no shallow (<12 km depth) earthquakes have occurred along the SWIF since the onset of instrumental recording.

[12] Evidence for one prehistoric earthquake comes from two coastal marshes straddling a strand of the SWIF on Whidbey Island [*Kelsey et al.*, 2004]. Sea level curves developed at each site show an abrupt change in relative sea level in the late Holocene. *Kelsey et al.* [2004] surmised from these observations that an earthquake occurred between 3200 and 2800 cal years B.P. along a strand of the SWIF concealed beneath a fold in Pleistocene sedimentary deposits on central Whidbey Island [*Kelsey et al.*, 2004]. Seismic data across the SWIF near the marshes show an asymmetrical syncline, with a steeper limb on the north side, developed in Quaternary glacial deposits. *Kelsey et al.* [2004] inferred that the syncline is cut by a steeply dipping fault. No evidence of deformed shorelines was found east of Whidbey Island where fault traces mapped using magnetic anomalies come ashore on the mainland.

3. Onshore Location of the SWIF

[13] Although the location of the SWIF is relatively well known on Whidbey Island and surrounding waterways, its projection and three-dimensional characteristics on the Washington mainland are poorly understood. If continued on strike to the southeast, the SWIF passes midway between the cities of Everett and Seattle (Figure 1b). *Johnson et al.* [1996] state that the SWIF extends beneath the northeast Seattle basin and possibly continues to the southeast. Because the SWIF has been active in Holocene time [*Kelsey et al.*, 2004], understanding the mainland segment is of considerable interest to earthquake hazard assessment.

3.1. Evidence From Aeromagnetic Anomalies

[14] High-resolution aeromagnetic anomalies provide important clues to help answer questions concerning the history and configuration of the SWIF. Figure 4a shows magnetic data acquired in 1997 as part of an aeromagnetic survey covering the entire Puget Lowland south of the Canadian border [*Blakely et al.*, 1999]. Magnetic measurements were recorded at an altitude of 250 m above ground or as low as safely possible; flight altitude averaged 262 m in the area of Figure 4a. Flight lines were directed north-south and spaced approximately 400 m apart; east-west tie lines were spaced 8 km apart. Two stationary magnetometers were operated continuously during the survey to measure and subsequently correct for transient magnetic fields. Total field measurements were reduced to anomaly values by subtraction of the International Geomagnetic Reference Field updated to the date of the survey.

[15] The study area includes two prominent magnetic anomalies lying along the southeastward projection of the SWIF, labeled A and B in Figure 4a. Part of anomaly A is located over mafic volcanic rocks exposed at Devils Butte and Bald Hill [*Yount and Gower*, 1991; *Minard*, 1985]), and it is likely that all of anomaly A is caused by these same volcanic rocks in the shallow subsurface. *Johnson et al.* [1996] considered these rocks to be equivalent to Eocene volcanic rocks of Mount Persis [*Tabor et al.*, 1993], correlative with Tukwila Formation exposed 30 to 40 km to the south. The volcanic rocks of Mount Persis, exposed at Devils Butte and Bald Hill, are the only significantly magnetic rocks exposed anywhere within the study area of Figure 4. However, these same volcanic rocks were encountered at 2.4 km depth in the Standard Oil Company of California Socal-Schroeder 1 well (Figures 4 and 5), located 4 km north of Lake Washington [*Rau and Johnson*, 1999]. Thus it is likely that volcanic rocks of Mount Persis, exposed at Devils Butte and Bald Hill, continue in the subsurface to the location of the Socal-Schroeder well and perhaps beyond. Consequently, we interpret the source of anomaly B to be an anticline within this Eocene volcanic unit.

[16] The linear northeastern margin of anomaly B (Figure 4a, label C) may reflect tectonic controls on this folded volcanic rock. Magnetic lineation C forms an obvious boundary between positive anomaly values to the south and negative anomaly values to the north (Figures 2 and 4). This linear gradient may reflect either an abrupt northeastern discontinuity or edge to the concealed volcanic rocks of Mount Persis or an abrupt change from normal to reverse magnetization. In either case, the linear nature of the gradient is consistent with a faulted contact.

[17] In addition to anomalies A and B, the onshore region exhibits a "noisy" mottled pattern, undoubtedly caused in part by man-made structures, especially in the urbanized region between Mukilteo and Lake Washington (Figure 4a). Superimposed on this mottled pattern are a number of short-wavelength, linear magnetic anomalies lying subparallel to

Figure 4. Aeromagnetic anomalies over the mainland region between Seattle and Everett. See Figure 2 for location. (a) Aeromagnetic anomalies. Arrows and labels A through D indicate magnetic anomalies discussed in text. SA and SS are Alderwood and Socal-Schroeder exploratory wells discussed in text and shown in Figure 5. GMS is location of ground magnetic survey. (b) Aeromagnetic anomalies processed in order to emphasize anomalies due to shallow sources. Black dashed and dotted lines are aeromagnetic lineaments interpreted to be part of a broad zone of SWIF deformation, dotted where less certain. Crosshatch pattern indicates zone of linear magnetic anomalies. White dotted lines are mapped location of SWIF strands offshore [*Johnson et al.*, 1996]. BL, Bothell lineament; CLL, Cottage Lake lineament; DLL, Devils Lake lineament; GL, Grace lineament; LBL, Lake Ballinger lineament; LL, Leota lineament; LBCL, Little Bear Creek lineament; KL, Kenmore lineament; WL, Woodinville lineament.

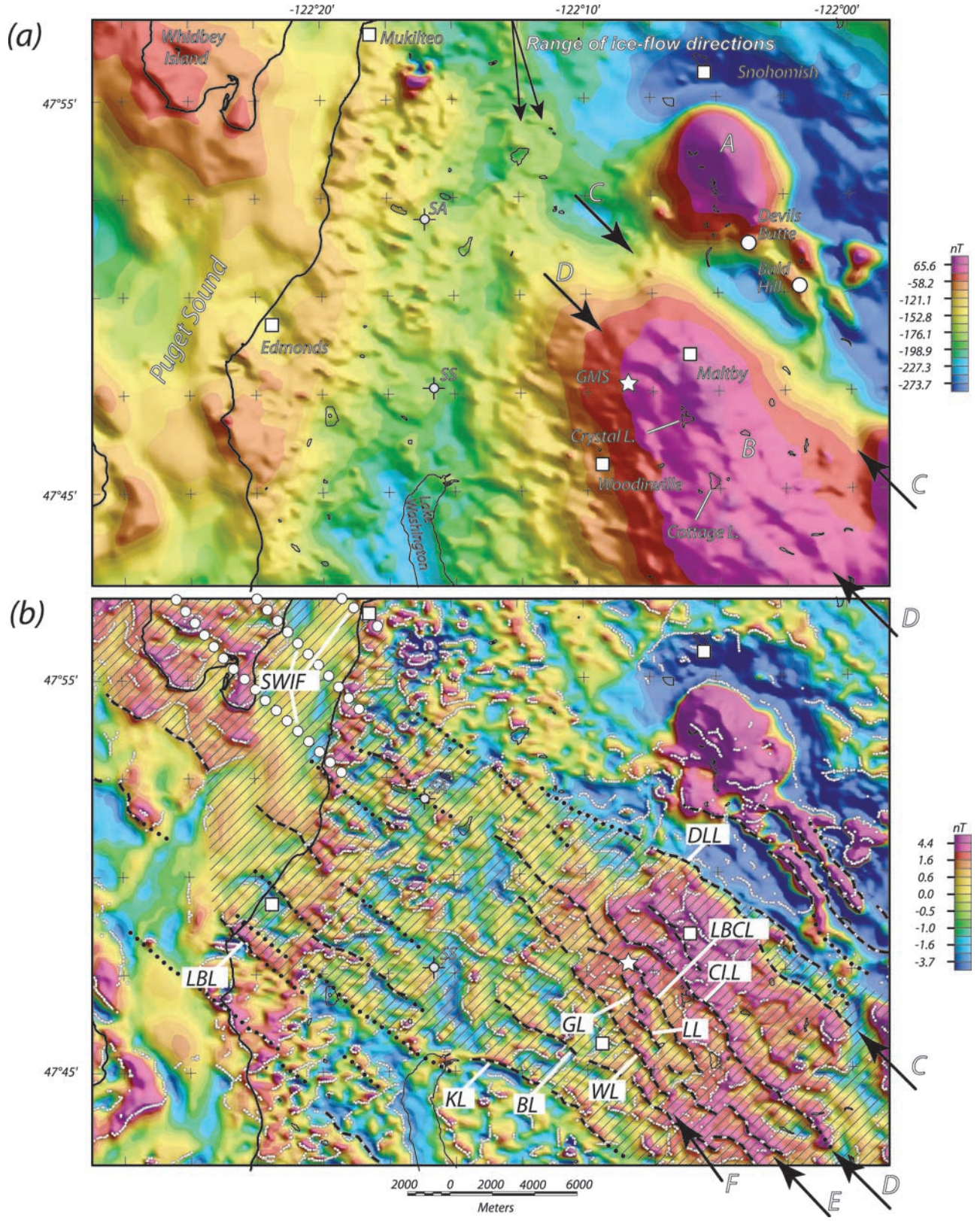

Figure 4

the onshore projection of the SWIF. The most prominent of these linear anomalies is superimposed on anomaly B and is labeled anomaly D on Figure 4a. Anomaly D and other magnetic lineaments in the study area extend for tens of kilometers, are not associated with highways or other linear man-made objects, and thus are unlikely to be caused by man-made construction. The orientation of the linear magnetic anomalies parallel with the onshore projection of the

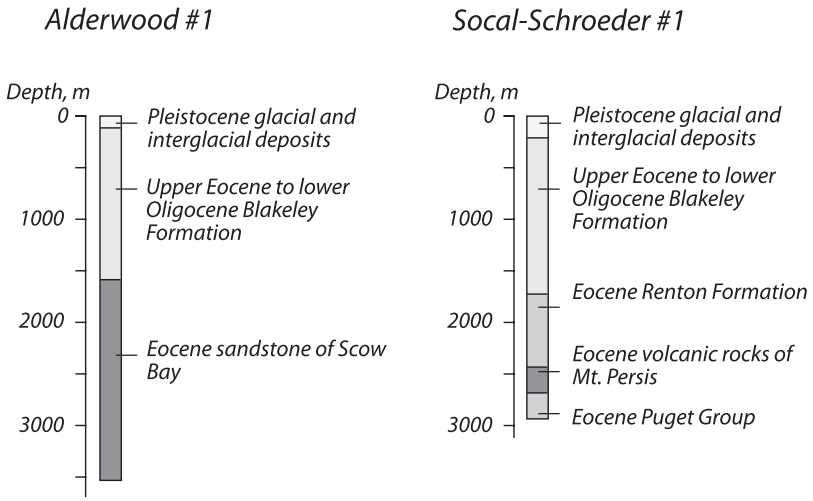

Figure 5. Lithologies encountered in two deep exploratory wells, generalized from *Rau and Johnson* [1999]. See Figure 4 for locations.

SWIF and oblique to the orientation of glacial transport suggests that the anomalies have tectonic origins.

[18] Figure 4b shows an attempt to highlight these subtle linear magnetic anomalies. The original magnetic data were analytically continued to a slightly higher altitude, 50 m above the original observation surface, and then subtracted from the original data. This two-step procedure emphasizes shallow sources at the expense of deeper sources [*Blakely et al.*, 2004]. Figure 4b also shows the location of magnetic contacts estimated automatically with a method described by *Blakely and Simpson* [1986].

[19] We have identified a number of northwest striking magnetic lineaments (dotted and dashed black lines, Figure 4b) lying within a broad zone 18 to 24 km wide. In following discussions, we will use local place names to identify specific aeromagnetic lineaments. Anomaly D will be referred to as the Cottage Lake lineament (label CLL, Figure 4b), which is well expressed as a semicontinuous feature extending at least 18 km. Other prominent magnetic lineaments in Figure 4b include the Devils Lake (DLL), Little Bear Creek (LBCL), Leota (LL), Grace (GL), Woodinville (WL), Bothell (BL), Kenmore (KL), and Lake Ballinger (LBL) lineaments.

[20] These low-amplitude magnetic anomalies over glacial deposits are most likely caused by the juxtaposition of weakly magnetic lithologies having slightly contrasting magnetic properties. From magnetic anomalies alone, we cannot determine whether the juxtaposition was caused by tectonic, depositional, or glacial processes. However, because all of these northwest trending magnetic lineaments align with the onshore projection of the SWIF and are oblique to glacial transport (Figure 4a), we consider the possibility that some of the anomalies reveal individual near-surface strands of the SWIF. Modeling experiments indicate that small, near-vertical offsets of subhorizontal, weakly magnetic layers produce anomalies comparable in amplitude and wavelength [*Blakely et al.*, 2004]. Thus, faults that offset weakly magnetic layers within the Pleistocene and younger section may be responsible for these anomalies. The sense of the anomalies suggests that these hypothetical faults would be northeast-side-down. Other explanations are possible, of course, and independent observations are required to elucidate the true origins of these linear anomalies. In following sections, we will describe compelling correlations between some of the aeromagnetic lineaments, lidar scarps, and high-resolution seismic reflection data that lend credence to a fault interpretation.

[21] Figure 4b shows additional northwest striking lineaments in the area northwest of Lake Washington. These lineaments are less distinctive than those discussed in section 3.1 and thus are indicated by dotted lines. Nevertheless, it is possible that these magnetic anomalies are caused by shallow faults. The strongest evidence comes from an east-west transect of 157 shallow boreholes (average depth 75 m) extending from Woodinville to Puget Sound [*McCormack*, 2003; *Yeats and St. Peters*, 2006]. These geotechnical boreholes showed soil disturbances at several magnetic anomalies that could be interpreted as tectonic in origin [*Blakely et al.*, 2004].

3.2. Lithologies Responsible for Linear Magnetic Anomalies

[22] The Cottage Lake aeromagnetic lineament and other linear magnetic anomalies in the study area have very short wavelengths in the direction normal to the lineation, with steepest gradients typically occurring over distances less than 1 km. Such sharp gradients require that the anomalies originate from within 1 km of the Earth's surface. The Cottage Lake aeromagnetic lineament is superimposed on broader wavelength anomaly B, presumably caused by volcanic rocks of Mount Persis, as discussed in section 3.1. The gradients associated with anomaly B, especially southeast of lineament C, are distributed over distances greater than several kilometers, suggesting that the source of anomaly B lies several kilometers below the surface in the area of the Cottage Lake aeromagnetic lineament. Thus, the source of the Cottage Lake aeromagnetic lineament and other linear magnetic anomalies in the area are caused by rocks or deposits that lie above the volcanic rocks of Mount Persis.

[23] Several observations suggest that near-surface sedimentary rocks and glacial deposits in this area could be sufficiently magnetic to produce low-amplitude magnetic

Table 1. Magnetic Susceptibility Measurements in the Woodinville-Maltby, Washington[a]

Location	Description	Susceptibility[b]	N[c]	Magnitude[d]
NE 160th St and 210th Ave NE	Pleistocene, Vashon recessional outwash	2.817	10	0.12
NE 159th St and 212nd Ave NE	Pleistocene, Vashon recessional outwash overlying till	1.832	10	0.08
NE 205th St	Pleistocene, Vashon till, some iron-oxide staining	1.367	10	0.06
NE 205th St	Pleistocene, Vashon till and advance outwash	1.335	10	0.05
NE 205th St	Pleistocene, Vashon proglacial deposit, fine-grained silty clay	2.405	8	0.11
Welch Rd near Elliott Rd	Blakeley Formation, fine-grained	0.225	10	0.01
Welch Rd near Elliott Rd	Blakeley Formation, pebbly	2.690	13	0.11
Welch Rd near Elliott Rd	Blakeley Formation, fine-grained	0.150	3	0.01
Elliott Rd near Fales Rd	Blakeley Formation, fine-grained	0.308	16	0.01
SR 522 near Bald Hill, site A	Mount Persis volcanic rocks, weathered	2.173	19	0.10
SR 522 near Bald Hill, site B	Mount Persis volcanic rocks, unweathered	16.894	14	0.75
Gravel pit, Snohomish-Monroe Rd	Mount Persis volcanic rocks, weathered	5.255	17	0.23
Quarry on Bald Hill	Mount Persis volcanic rocks, unweathered	16.160	10	0.71

[a]All measurements conducted with a handheld Model KT-6 Kappameter manufactured by Geofyzika.
[b]Average susceptibility in SI units; displayed numbers multiplied by 103.
[c]Number of individual measurements.
[d]Magnetization in A/m.

anomalies at aeromagnetic altitudes. Sandstone and siltstone of the upper Eocene to lower Oligocene Blakeley Formation observed within the Alderwood 1 well (Figure 5, left) were described as commonly tuffaceous [*Rau and Johnson*, 1999] and thus may be weakly magnetic. We confirmed this conjecture with in situ magnetic susceptibility measurements (Table 1) of four bedrock exposures in the Maltby area mapped as Blakeley Formation [*Minard*, 1985]. Fine-grained exposures had an average induced magnetization of only 0.01 A/m, but one pebble bed had an average induced magnetization of 0.11 A/m. Moreover, in situ magnetic susceptibility measurements of Vashon age recessional outwash and older Pleistocene glacial deposits in the Woodinville-Maltby area (Table 1) exhibited induced magnetizations ranging from 0.05 to 0.12 A/m, with an overall average value of 0.09 A/m. Although weak, these magnetizations are sufficient to produce low-amplitude magnetic anomalies at low altitudes.

3.3. Ground Magnetic Survey

[24] An open field near Woodinville (Figure 4a, label GMS) afforded an excellent opportunity to conduct a ground magnetic survey over Pleistocene glacial deposits in a region characterized by the linear aeromagnetic anomalies. This open field is traversed by the Little Bear Creek lidar scarp (discussed section 3.4) and the Little Bear Creek aeromagnetic lineament (Figure 4b, label LBCL) and was the site of the Beef Barley trench (discussed section 4.4). The open field was ideal for this type of investigation: it was devoid of significant metallic objects that adversely influence magnetic measurements, and the lack of tree cover facilitated accurate GPS navigation. Profiles were conducted on foot while carrying a portable cesium vapor magnetometer and GPS system. Seventeen subparallel profiles were directed northeast; a single tie line was oriented northwest. A stationary proton precession magnetometer was operated continuously during the survey in order to record and subsequently to correct for time-varying magnetic fields.

[25] Figure 6a shows the results of the ground magnetic survey. Magnetic field measurements along each profile were corrected for time-varying magnetic fields and then interpolated to a rectangular grid. Individual anomalies typically range between −40 and +20 nT and have gradient widths on the order of a few tens of meters. Individual, isolated anomalies measured at ground level with these characteristics would not be observable at aeromagnetic altitudes, but widespread clusters of similar anomalies may coalesce to form aeromagnetic anomalies.

[26] The ground magnetic anomalies are small in amplitude, especially considering they were measured only 2 m above the ground. Nevertheless, we are struck by the linear nature of these anomalies and their orientation parallel to the Little Bear Creek aeromagnetic anomaly, the Little Bear Creek lidar scarp, and the onshore projection of the SWIF. The anomalies are oblique to the direction of glacial transport, and we suggest that these anomalies reflect faulted contacts in the shallow subsurface.

[27] The sharp gradients of the linear ground magnetic anomalies indicate that their sources lie at shallow depth. To quantify this assertion, we applied a simple graphical technique to anomaly GA as recorded along profiles 6 and 8 (Figures 6b and 6c). The technique, known as the Peters method [*Peters*, 1949; *Blakely*, 1995], capitalizes on the relationship between source depth and anomaly gradient. We estimate that the source of anomaly GA lies at a maximum depth of 8 to 20 m below ground level. Geotechnical boreholes in the immediate vicinity of the Beef Barley trench (discussed in section 4.4) indicate that Pleistocene glacial deposits extend to depths of about 100 m

Figure 6. Ground magnetic survey of a site near Woodinville, Washington. See Figure 4 for location. (a) Ground magnetic anomalies. Rainbow colors are magnetic anomaly values gridded from measurements taken along semiparallel profiles (solid black lines). Profiles 6 and 8 highlighted. Dotted black lines indicate northwest striking gradients discussed in text. GA is gradient used to estimate source depth. Bold dashed line is location of Little Bear Creek lidar lineament. Blue line is approximate location of Beef Barley trench discussed in text. (b) Profile 6. Dashed and dotted lines show elements of an estimation of source depth, known as Peters method. See *Peters* [1949], *Blakely* [1995], or *Sherrod et al.* [2005a] for details of this methodology. (c) Profile 8.

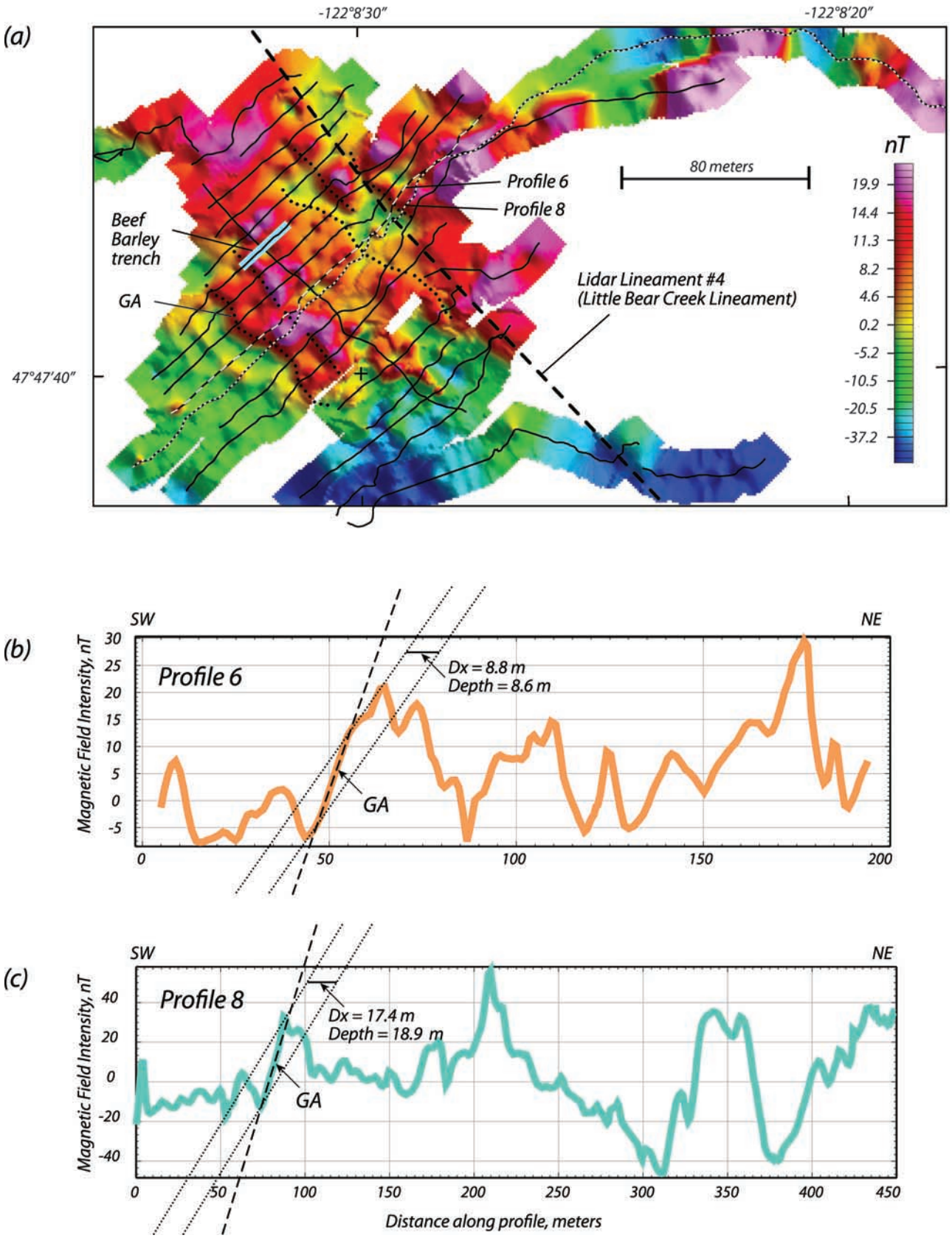
(a)
-122°8'30"
-122°8'20"
47°47'40"
80 meters
nT
19.9
14.4
11.3
8.2
4.6
0.2
-5.2
-10.5
-20.5
-37.2
Profile 6
Profile 8
Beef
Barley
trench
GA
Lidar Lineament #4
(Little Bear Creek Lineament)
(b)
SW
NE
Profile 6
Dx = 8.8 m
Depth = 8.6 m
GA
Magnetic Field Intensity, nT
30
25
20
15
10
5
0
-5
0
50
100
150
200
(c)
SW
NE
Profile 8
Dx = 17.4 m
Depth = 18.9 m
GA
Magnetic Field Intensity, nT
40
20
0
-20
-40
0
50
100
150
200
250
300
350
400
450
Distance along profile, meters

Figure 6

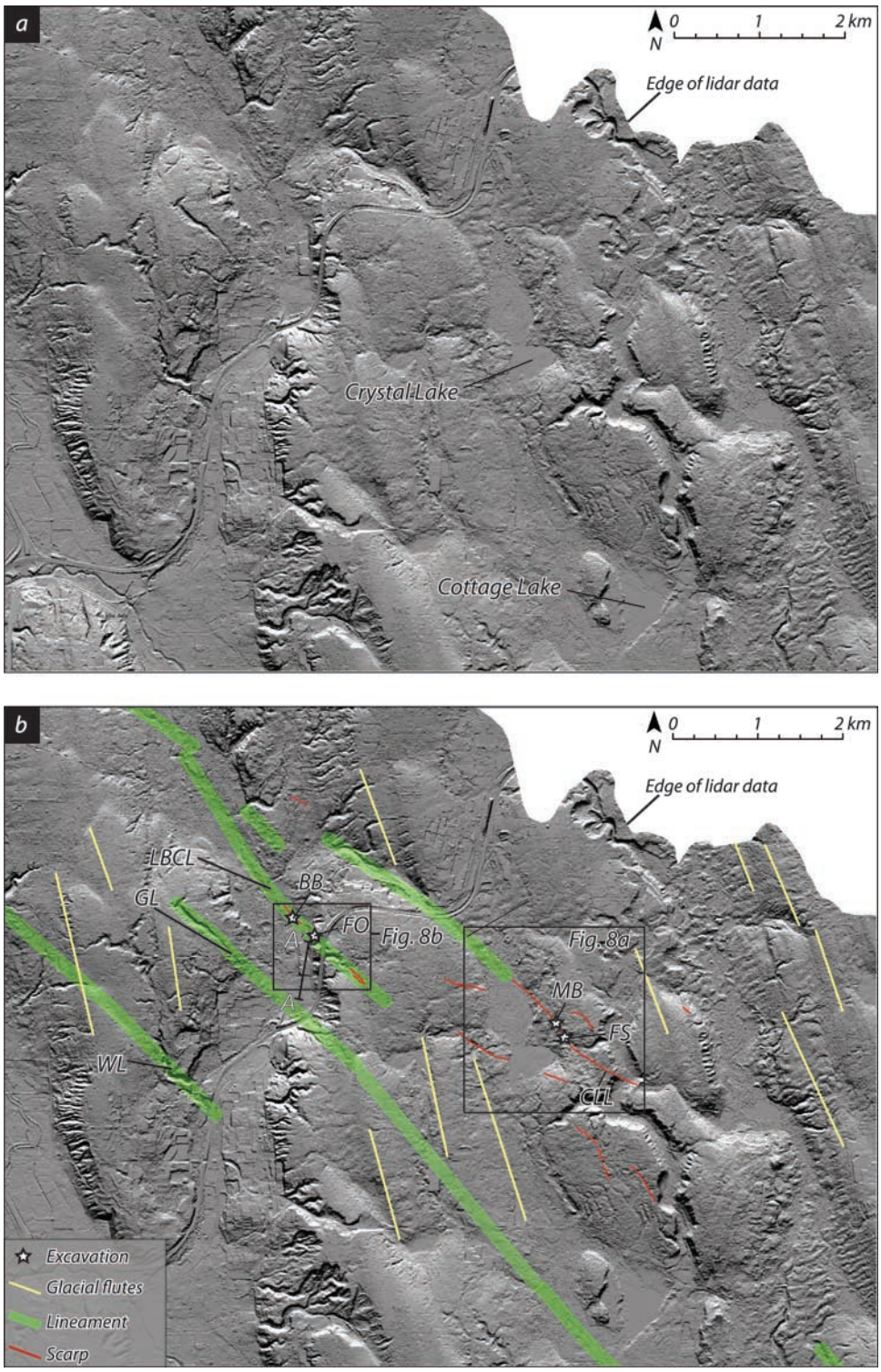

Figure 7. (a) Uninterpreted bald Earth lidar image of the Cottage Lake and Little Bear Creek lineaments. (b) Interpreted bald Earth lidar image of the Cottage Lake and Little Bear Creek lineaments. Thick green lines are topographic lineaments, and thin red lines are lidar scarps. The line marked A-A′ indicates the location of a cross section shown in Figure 11.

beneath the open field [*Aspect Consulting*, 2005]. Specifically, boreholes encountered glacial till, overlain by outwash, at depths increasing west-southwestward across the trench site [*Aspect Consulting*, 2005]. Extrapolating from these boreholes, we estimate the glacial till to lie approximately 10 m below ground level at ground magnetic anomaly GA, roughly consistent with the magnetic source depth (8 to 20 m) estimated from the Peters method.

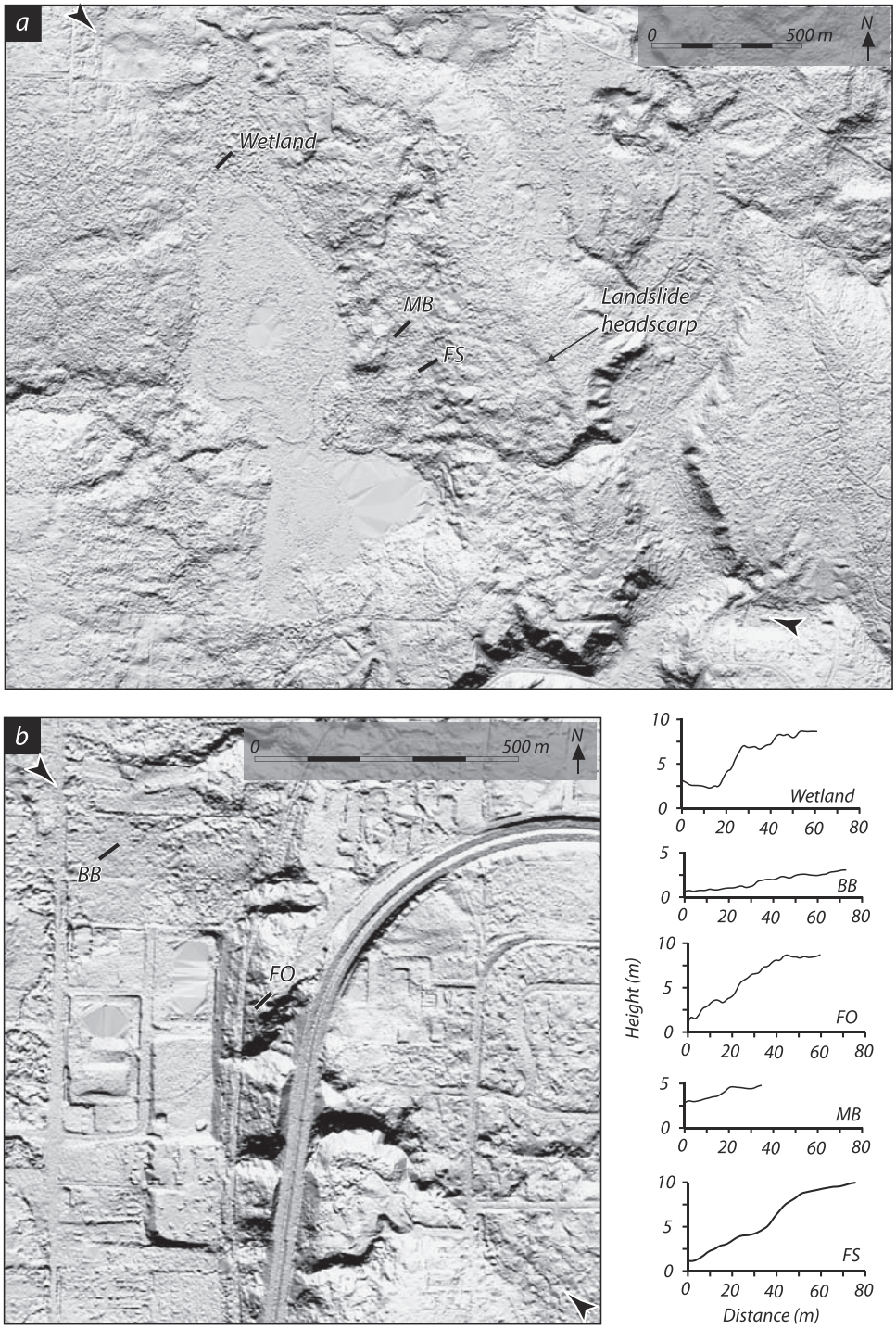

Figure 8. (a) Lidar image of the area around Crystal Lake showing the locations of the Mountain Beaver (MB) and Flying Squirrel (FS) excavations. Arrows point at each end of the scarp. Small lines indicate the locations of topographic profiles created using lidar data. (b) Lidar image of the area surrounding the Beef Barley (BB) and French Onion (FO) excavations. Arrows point at each end of the Little Bear Creek lineament, and small lines indicate the locations of topographic profiles created using lidar data. (bottom right) Topographic profiles using lidar data are located and are referenced to the locations shown on Figures 8a and 8b.

Furthermore, anomaly GA is 300 m northwest of and on trend with a discontinuity identified in geotechnical boreholes, marked by a change from thick layers of silt and clay to the northeast, presumably lake deposits correlative with those in the French Onion trench nearby (discussed in section 4.5), and silty sands with variable amounts of gravel to the southwest [*Yeats and St. Peters*, 2006].

3.4. Correspondence of Magnetic Anomalies and Lidar Features

[28] Lidar mapping near Woodinville reveals several linear features along the onshore projection of the SWIF concentrated in the area near Crystal Lake (Figures 7 and 8; see Figure S1 in the auxiliary material[1]). The most prominent features observed on the lidar images are glacial flutes. Glacial flutes are linear topographic features created by flowing ice and subglacial meltwater. Two ice flow trends are observed in the study area, one roughly north to south (azimuth of ~175°) in the western part of the study area, and a second oriented slightly southeast (azimuth of ~165° to ~160°) in the eastern part of the study area. These former ice flow directions are important because topographic features that cut across the flutes at high angles are likely not related to glacial flow and may reflect postglacial processes.

[29] Other features observed in the lidar data are more subtle than the glacial flutes (Figure 8). These features consist mainly of short (<1 km), northeast-side-up scarps and longer topographic lineaments (approximately 0.5 to 4 km long). The scarps and lineaments fall close to, or directly on, low-amplitude linear magnetic anomalies also on strike with the SWIF (Figure 4) and are oblique to the predominant trend of glacial grooves and flutes [*Blakely et al.*, 2004]. Without independent information, linear magnetic anomalies can be ascribed to a variety of geologic sources. However, the coincidence of linear magnetic anomalies with scarps and topographic lineaments suggests a tectonic origin. Specifically, we suggest that the Cottage Lake and Little Bear Creek aeromagnetic anomalies (Figure 4b) reveal strands of the SWIF in the shallow subsurface, where recent faulting has created subdued scarps and topographic lineaments on the land surface.

[30] A northeast-side-up scarp lying along the Cottage Lake aeromagnetic lineament is the most prominent scarp observed in the lidar data (Figure 8a). This north-side-up scarp, located east of Crystal Lake, is about 3 km long and between ~1.5 and 4 m high. Poor lidar returns in dense vegetation obscure the scarp morphology along its southeast end. A second topographic feature identified on the lidar maps (Figure 8b) lies on strike with the Little Bear Creek aeromagnetic lineament (Figure 4b) and close to a shallow magnetic anomaly identified in our ground magnetic survey (Figure 6). This topographic feature, called the Little Bear Creek scarp, follows Little Bear Creek and consists of several aligned ravines and scarps. To investigate whether the Cottage Lake and Little Bear Creek lineaments lie along active faults, we excavated trenches across the scarps to examine glacial and postglacial soils for evidence of recent deformation.

4. Paleoseisimology of the SWIF

[31] Fault scarp excavations and published coastal marsh studies provide the basis for developing a history of Holocene earthquakes on the SWIF. We excavated four trenches across two lidar scarps to test the hypothesis that the scarps and coincident magnetic anomalies are due to movement along shallow faults. These excavations, named Mountain Beaver, Flying Squirrel, Beef Barley, and French Onion, are discussed here. The locations of the excavation sites are shown in Figures 7b and 8. Details of these and other excavations are presented in detail by *Sherrod et al.* [2005a, 2005b]. Published studies of coastal marsh stratigraphy at two widely separated locations along the SWIF provide additional information on the timing of previous seismic events [*Kelsey et al.*, 2004; *Bourgeois and Johnson*, 2001].

4.1. Methods

[32] Stratigraphic and structural observations collected from four excavations yield insights into past earthquakes along the SWIF. We excavated two trenches (named Mountain Beaver and Flying Squirrel) across the Cottage Lake lineament where a scarp observed on lidar maps coincides with aeromagnetic anomalies (Figure 9). Two excavations crossed the Little Bear Creek lineament, one in recessional outwash filling the Little Bear Creek valley (named Beef Barley) and the second on the edge of a bluff overlooking the valley (named French Onion; Figure 10). In each excavation, we specifically looked for evidence of past surface ruptures from folding and faulting. Evidence for strong shaking at each site, in the form of liquefaction features, was also mapped. At sites along the Cottage Lake lineament, we observed evidence for past folding and faulting, and at sites along the Little Bear Creek lineament we observed evidence for past folding, faulting, and liquefaction. In the following discussion we refer to events and folding repeatedly. Our use of these terms reflects seismic events unless specifically noted.

[33] Samples for radiocarbon analyses using atomic mass spectrometry (AMS) consisted of detrital charcoal samples collected from two of the excavations. The remaining two excavations did not yield suitable samples for analysis. We report conventional radiocarbon ages as ^{14}C years B.P. We used the computer program OxCal [*Ramsey*, 1995] and the INTCAL98 calibration data of *Stuiver et al.* [1998] to calibrate the reported ages; the 95% confidence interval of each calibrated age is reported as cal years B.P. (before A.D. 1950). We also refer to rounded ages for events as occurring years before A.D. 2000; thus, a calibrated age of 900 cal years B.P. is about A.D. 1100.

[34] Ages of two units from the Mountain Beaver excavation were estimated by radiocarbon dates on clasts of detrital charcoal. A well-rounded clast of charcoal from recessional outwash deposits yielded an AMS radiocarbon age of 31,330 ± 340 ^{14}C years B.P. (sample BETA-194042). A charcoal clast collected from the middle of a buried soil horizon yielded an AMS radiocarbon age of 10,190 ± 40 ^{14}C years B.P. (sample BETA-194043; 12,090–11,670 cal years B.P.). The age of the sample from recessional outwash suggests that the charcoal was likely recycled and incorporated into younger outwash deposits during deglaciation. The age of the sample from the buried soil suggests that a forest soil developed on glacial deposits in the early Holocene and was subsequently buried by colluvium.

[35] The only material recovered for radiocarbon dating from the Beef Barley excavation was retrieved from the base of a sandy loam (Figure 10a). Charcoal samples collected at the base of the soil yielded AMS ages of 2450 ± 40 ^{14}C years B.P. (sample BETA-200523; 2730 to

[1]Auxiliary materials are available in the HTML. doi:10.1029/2007JB005060.

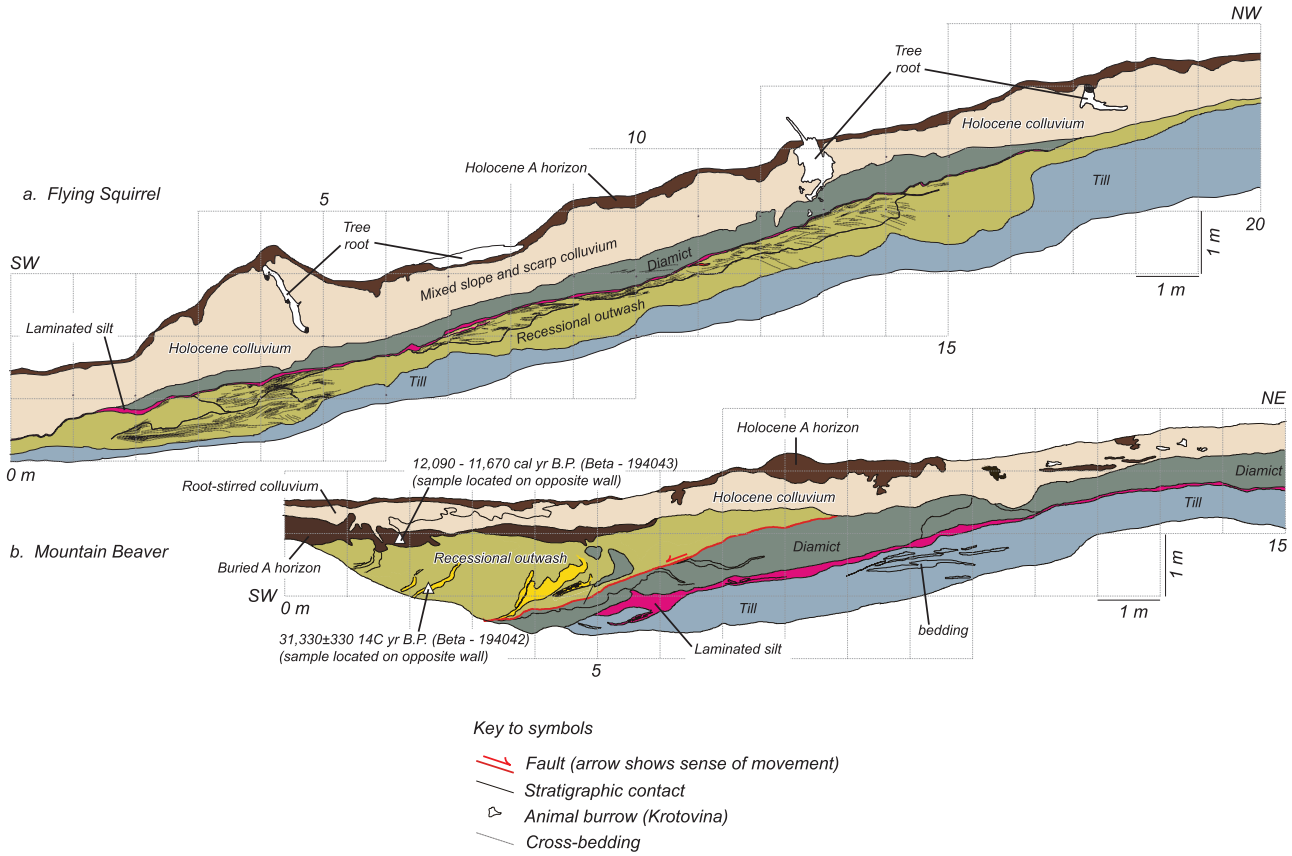

Figure 9. Excavations across the Cottage Lake lineament. (a) Simplified excavation log of the Flying Squirrel trench (west wall). Log is flipped horizontally relative to actual mapped log. (b) Simplified excavation log of the Mountain Beaver trench (east wall). Unit designations shown are identical to those mentioned in the text.

2350 cal years B.P.) and 2660 ± 50 ^{14}C years B.P. (sample BETA-200524; 2850 to 2740 cal years B.P.).

4.2. Flying Squirrel Excavation

4.2.1. Stratigraphy

[36] The Flying Squirrel excavation was 20 m long and was placed across a 3.5−m high, north-side-up scarp on a forested slope (Figure 9a). Till was exposed at the base of the stratigraphic section and consisted of a gray sandy loam with faceted pebbles and cobbles of mainly felsic and intermediate volcanic rocks. An erosional unconformity separated the till from overlying recessional outwash deposits, which consisted primarily of gravelly fine to coarse sand to sandy gravels. Cross-bedded sands were interbedded with the gravelly deposits. A silt layer with thin, planar lamination capped the recessional outwash deposits. The silt dips from about 10° to ~35° [*Sherrod et al.*, 2005a]. The laminated silt is overlain by a diamict, consisting of a gray, pebbly sandy loam with planar and cross stratification observed in several places and interpreted as an ablation till or debris flow. A thick, reddish-brown sandy loam to loam, with weak subblocky pedogenic structures and scattered pebbles and cobbles, capped the entire section, and is interpreted as mixed slope and scarp colluvium. Tree roots and burrows of *Aplodontia ruppia* (Mountain Beaver) extended downward from the ground surface into the colluvium. A thin layer of organic detritus laid over the colluvium and mantled the ground surface.

[37] We did not recover organic material from the excavation suitable for radiocarbon analysis. Therefore, we rely on maps and our observations for age estimates of the deposits. Geologic maps of the area surrounding our excavations show the surficial deposits as Vashon outwash and till and our excavations penetrated only the upper few meters of these deposits [*Booth et al.*, 2004, http://geomapnw.ess.washington.edu]. Sediments overlying the till were not overconsolidated, suggesting that the deposits are postglacial in age because they were not overridden by glacial ice.

4.2.2. Deformation History

[38] The Flying Squirrel excavation across the Cottage Lake lineament did not yield clear evidence for past fault movement: no fault was observed in the excavation. However, observations consistent with folding and the presence of the lidar scarp point to at least one past earthquake. Several observations in the excavation suggest that the glacial deposits were folded beneath the scarp. First, the thinly laminated silt layer dipped up to ~35°, too high for a deposit assumed to be paleohorizontal. Second, the entire depositional package was warped across the scarp, suggesting that folding occurred after the Vashon glacier retreated from the area. The observed folding accounts for all of the measured scarp height, suggesting that one event could

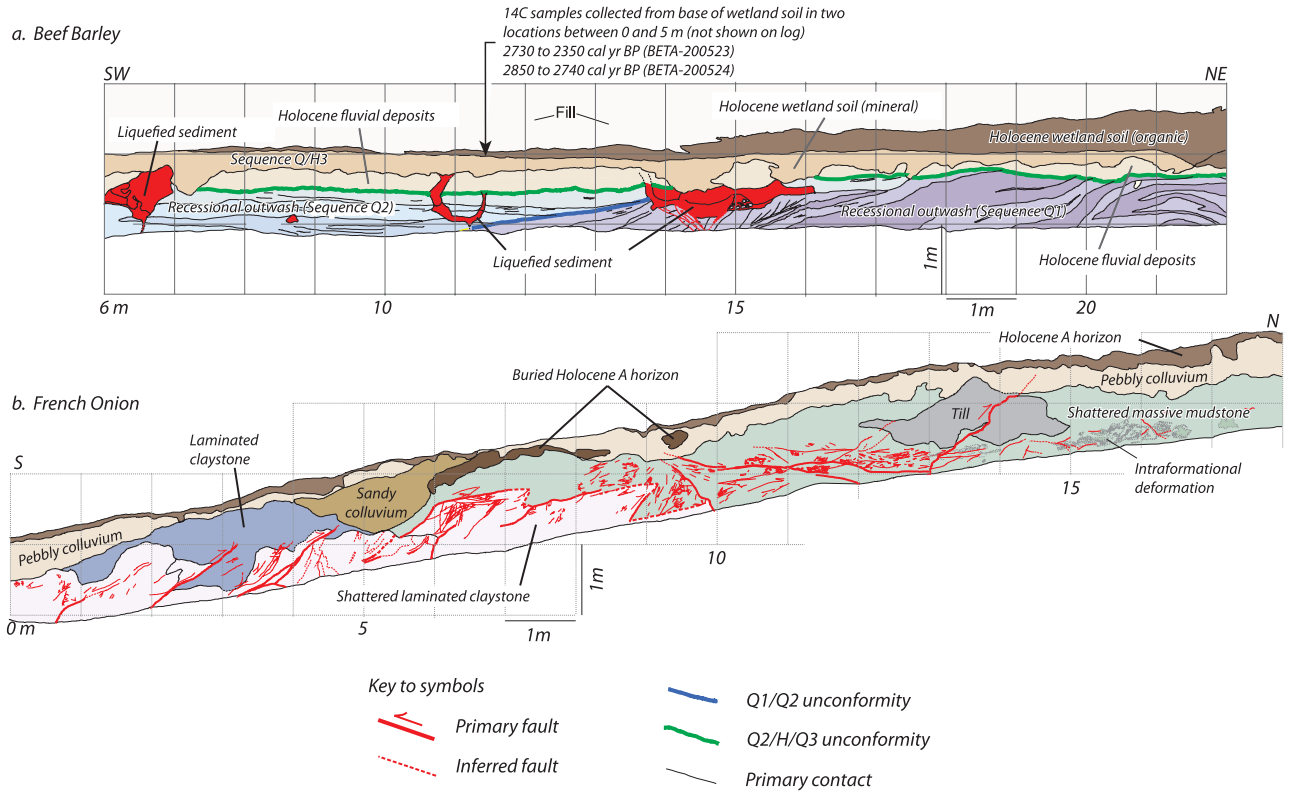

Figure 10. Excavations across the Little Bear Creek lineament. (a) Simplified excavation log of the Beef Barley trench (west wall). (b) Simplified excavation log of the French Onion trench (east wall). Excavation log is flipped horizontally to allow easier comparison of logs.

explain both the scarp and observed deformation in the excavation.

4.3. Mountain Beaver Excavation

4.3.1. Stratigraphy

[39] A second excavation along the Cottage Lake lineament, named the Mountain Beaver site, consisted of a 16-m-long excavation across a ~1.5-m-high scarp lying along the Cottage Lake aeromagnetic lineament (Figure 9b). This excavation exposed glacial till at the base of the excavation, consisting of dense gray sandy silt with faceted pebbles and cobbles. We used small silt and sand interbeds to estimate the dip of the till (Figure 9b). Overlying the till was a thin layer of compacted silt, laminated in places. The silt was in turn overlain by a pebbly diamict consisting of dense sandy silt with abundant faceted pebbles and cobbles and scattered stratified sand layers.

[40] A low-angle fault separated the pebbly diamict from overlying recessional outwash deposits. The fault truncated and deformed sand and silt layers in the pebbly diamict such that a normal sense of movement on the fault was clearly observed. Above the fault, a sequence of massive to interbedded sand and pebbly silty sands (recessional outwash) pinched out toward the middle of the trench wall. We could not determine if the fault offset younger deposits above the outwash so we arbitrarily stopped the fault at the contact between the outwash and overlying colluvium. A buried A horizon and buried weak B horizon were developed in the top of the recessional outwash deposits. Small gravel lenses (not shown in Figure 9b) and silty colluvial deposits bury the former A horizon. Surface accumulations of modern forest litter mantled the top of the exposure, with thicker accumulations near the base of the scarp.

4.3.2. Deformation History

[41] Dipping laminated silt layers, deformed recessional outwash deposits, and a buried soil in the Mountain Beaver excavation indicated postglacial tectonic folding along the Cottage lake lineament. Dips on laminated silt layers and thin beds of sand suggest some postdepositional warping (Figure 9b) [*Sherrod et al.*, 2005b]. Folding in the Mountain Beaver excavation is also indicated by dips mirrored in the till and recessional outwash deposits, and in the contacts between units, suggesting that a single earthquake warped the entire section. The silt layer geometry and contacts between stratigraphic units indicated that warping was greater than 2 m. Lidar profiles across the scarp show that the present-day scarp height is between 2.5 and 4 m. Over time, the original scarp at the Mountain Beaver site degraded and colluvium buried the former soil at the base of the scarp (Figure 8b). Radiocarbon ages from charcoal in the buried soil horizon provide a maximum age for the timing of the folding event described above. A single radiocarbon age from a sample collected near the middle of the buried soil yielded an age of 12,090–11,670 cal years B.P. This single age indicates that the folding event at the Mountain Beaver site occurred after 11,670 cal years B.P.

[42] The low-angle fault observed in the excavation is best explained as a mass-wasting feature, but an earthquake-related origin cannot be completely ruled out. The Mountain Beaver sites sits within a large, low angle landslide, and

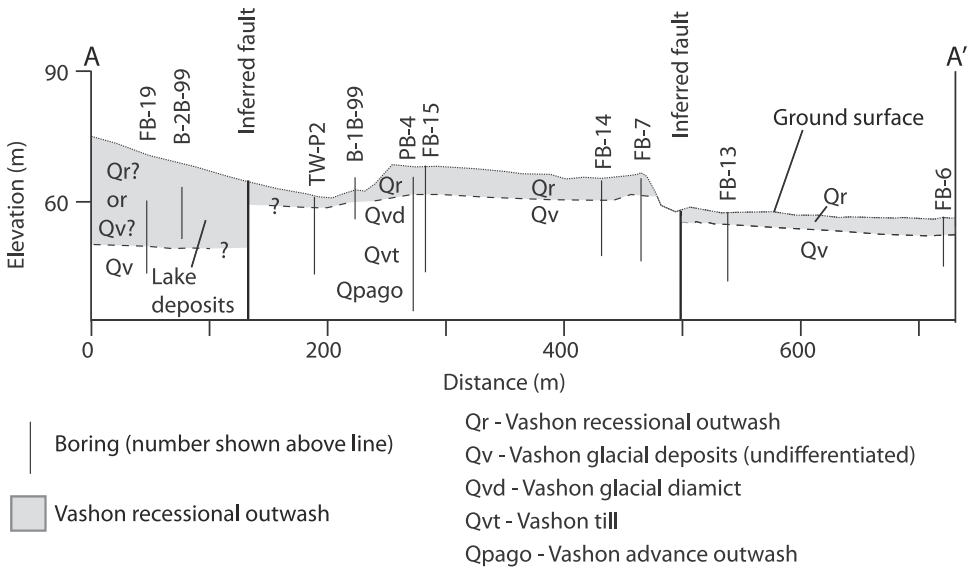

Figure 11. Geologic cross section based on geotechnical borings near the Beef Barley and French Onion excavations [*Yeats and St. Peters*, 2006]. Location of cross section is shown on Figure 7b (indicated as A-A′). The cross section shows that recessional outwash deposits cover the top of the entire section across the valley bottom. The Beef Barley excavation and the excavation shown in Figure 13 are placed in the uppermost part of the cross section. Preglacial deposits are not shown but were observed in other borings nearby [*Yeats and St. Peters*, 2006].

lidar maps show the scarp cutting across the landslide. This relationship, together with the stratigraphy suggests a simple sequence of events. First, a postglacial landslide caused soft sediment deformation of the recessional outwash deposits and created the low angle faulting observed in the excavation. After landsliding, an earthquake on a fault associated with the Cottage Lake aeromagnetic lineament folded the entire section exposed in the trench and created the scarp. The scarp cuts across the landslide and continues across the landscape into areas unaffected by mass wasting, showing that the scarp is younger than the landslide.

4.4. Beef Barley Excavation

4.4.1. Stratigraphy

[43] The Beef Barley excavation (Figure 10), located in the valley bottom of Little Bear Creek, was ~30 m long, ~2.4 m deep, and oriented N55°E across part of the Little Bear Creek topographic lineament. Geotechnical borings throughout the area surrounding the excavation identified a section of preglacial and glacial deposits typical of the Seattle region: preglacial lacustrine deposits at the base of the section, advance outwash and till in the middle, and recessional outwash at the top (Figure 11) [*Yeats and St. Peters*, 2006]. The Beef Barley excavation penetrates only the uppermost part of the recessional outwash deposits and Holocene alluvium. The deposits exposed in the excavation are best described as three sequences separated by unconformities (sequences Q1, Q2, and Q/H3). Sequence Q1 consists of yellowish brown to olive brown pebbly sand, loamy sand, and sandy loam. Locally, gravel beds within this sequence dipped ~36° to the SSW, while thin silts and clay layers dip as much as 22° to the SSW [*Sherrod et al.*, 2005b]. An angular unconformity (Q1–Q2 unconformity; thick blue line on Figure 10a) separates sequence Q1 from an overlying sequence of outwash deposits (sequence Q2). Sequence Q2 consists of yellow brown to olive gray gravelly sandy loam, sandy loam, sandy clay, and clay. We interpret sequences Q1 and Q2 as recessional outwash deposits because they overlie till observed in nearby borings and they lack overconsolidation typical of advance outwash [*Yeats and St. Peters*, 2006].

[44] A second unconformity separates sequence Q2 from an overlying gravelly deposit (Q2–Q/H3 unconformity; thick green line on Figure 10a). This unconformity was flat lying (between 8 and 16 m on Figure 10a) and rose slightly at the north end of the excavation, possibly as a result from the unconformity being slightly angular.

[45] Sequence Q/H3 lies above the Q2-Q/H3 unconformity and consisted of sandy gravels, sandy soils, and organic soils. Immediately overlying the unconformity was an olive brown sandy loam (labeled as Holocene fluvial deposits on Figure 10a). This unit spanned the length of the excavation but thinned considerably in the northeastern part of the excavation. Dark brown organic-rich sandy loam capped the sandy gravel and most likely represents prehistoric and historic surface soil developed at the site. Radiocarbon ages from detrital charcoal collected at the base of the sandy loam shows that the wetland deposits are a maximum of 2850 years old (sample BETA-200523; Figure 10a).

4.4.2. Deformation History

[46] Observation from the Beef Barley excavation suggests postglacial deformation and strong ground shaking. One, possibly two angular unconformities, and reverse faulting suggest multiple episodes of surface deformation. Liquefaction features observed throughout the excavation disturb recent soils and indicate strong ground shaking at the site in the late Holocene.

[47] The angular unconformity between sequences Q1 and Q2 marked the oldest period of deformation in the Beef Barley excavation (Figure 10a). Although no material was found to date either recessional outwash sequence, lithologic comparisons to other exposures and the lack of overconsolidation suggest that the unconformity separates two sequences of Vashon recessional outwash (~16,000 years old). We speculate that the unconformity was created when an earthquake on the Little Bear Creek lineament caused folding of sequence Q1. After the event, the folded units were beveled off by flowing water, and sequence Q2 was deposited. Thus, if tectonic folding created the Q1/Q2 unconformity, the unconformity represents an event during deglaciation and deposition of recessional outwash. Alternatively, the folding could represent glaciotectonism.

[48] A possible younger event occurred in either the latest Pleistocene or early Holocene, marked in the Beef Barley excavation by the unconformity between sequence Q2 and unit H/Q3. This unconformity could be the result of folding on the Little Bear Creek lineament, or, alternatively, the unconformity could be the result of normal fluvial processes acting at the site at the time of deposition. Neither alternative can be dismissed based on the data collected in the excavation. If the unconformity is the result of folding on the Little Bear Creek lineament, no age data exist to constrain the age of the event beyond being younger than ~12,000 years B.P and older than ~2850 cal years B.P., the maximum age of the wetland soils.

[49] The youngest event recorded in the Beef Barley excavation included slight folding, reverse faulting, and liquefaction. Evidence for folding is best seen between 14 and 20 m on the excavation logs [*Sherrod et al.*, 2005b] (Figure 10a). Good piercing points to measure displacement during this youngest event are lacking but the folding probably did not exceed tens of centimeters, and the faulting is likely limited to about 30 cm or less. However, none of these estimates account for lateral displacement, so total slip could have been significantly larger.

[50] Liquefaction accompanied the folding and faulting of the youngest event. Numerous liquefaction features were observed throughout the excavation, including sand-filled dikes injected upward through fine-grained facies of sequences Q1 and Q2 (Figure 10a). Parts of Q1 and Q2 entrained by flowing sand include blocks of silt in a large liquefaction feature located between 13.5 and 16 m on the excavation log. The liquefaction is associated with reverse faults observed between 14 and 15 m, suggesting that the faulting and liquefaction likely occurred during the same event.

[51] That the liquefaction is young is evidenced by the degree to which the wetland soil is disturbed by it. Holocene fluvial deposits and wetland soil were deformed into hummocks and swales above the liquefaction features, and one sand dike was observed cutting through the wetland soils. Since the liquefaction disturbed the youngest units exposed in the excavation, the events that caused the shaking had to postdate the youngest charcoal collected from the wetland soils, or about 2730 cal years B.P. It is possible that several events in the late Holocene caused strong ground shaking at the Beef Barley site. *Bourgeois and Johnson* [2001] documented at least three episodes of liquefaction in the late Holocene at the Snohomish River delta, about 26 km NNW of the site.

4.5. French Onion Excavation

4.5.1. Stratigraphy

[52] A small excavation was placed across the Little Bear Creek topographic lineament at the top of a bluff east of the Beef Barley excavation (Figure 10). This excavation, named French Onion, exposed glaciolacustrine claystones, till, colluvial deposits, and Holocene soils [*Sherrod et al.*, 2005a, 2005b]. The oldest units found in the French Onion excavation were mudstones and claystones interpreted as Late Pleistocene glacial lake deposits overidden by the last glacial advance into the Puget lowland (Figure 10b). A brown to gray, laminated claystone and a brown, massive mudstone found at the base of the exposed section had an autoclastic texture. In the south end of the excavation, a massive to laminated, gray claystone found above the fractured claystone/mudstone was not as intensely fractured. Near the north end of the excavation, a small lens of glacial till wall is seemingly surrounded by mudstone on three sides. All of these units were slightly indurated, possibly as a result of overconsolidation beneath a thick glacier. No materials for radiometric dating were observed in the glacial deposits, but the observed overconsolidation is consistent with deposits from an earlier glacial advance that were subsequently overridden during the last glacial advance (>16,400 years old [*Porter and Swanson*, 1998]).

[53] Above the overconsolidated glacial deposits is a buried soil and a pebbly colluvial deposit. The buried soil, a thick layer of buried organic-rich sandy loam to loam, lies directly on the shattered massive mudstone in the middle of the excavation. Immediately overlying this buried soil horizon are two correlative colluvial deposits. One colluvium consists of a sandy loam to loam with varying contributions of charcoal and pebbles of the underlying mudstone (labeled pebbly colluvium on Figure 10b). The mudstone pebbles were likely derived upslope from weathering of the older claystones. The second colluvium resembles the first except that it does not contain many mudstone pebbles (labeled pebbly colluvium on Figure 10b). A dark brown organic detritus layer caps the stratigraphic section.

4.5.2. Deformation History

[54] Fractures, faults, and shear zones in the French Onion excavation suggest a complex deformation history. We observed three structural fabrics in the excavation, one dipping southward, another dipping northward, and a third subhorizontal. When viewed in outcrop, these fabrics gave the older glacial units a shattered appearance. We observed each fabric in the older glacial deposits and traced only a few faults into the overlying Holocene units. However, it was not possible to determine if the faults actually offset the Holocene units or if the Holocene units were simply weathered into one of the older faulted units. With few exceptions, we could not determine the sense of motion of any of the faults.

[55] The south dipping fabric in the French Onion excavation contained several faults with reverse motion (Figure 10b). One of the south dipping reverse faults cuts a late Pleistocene till. Several south dipping faults appeared to

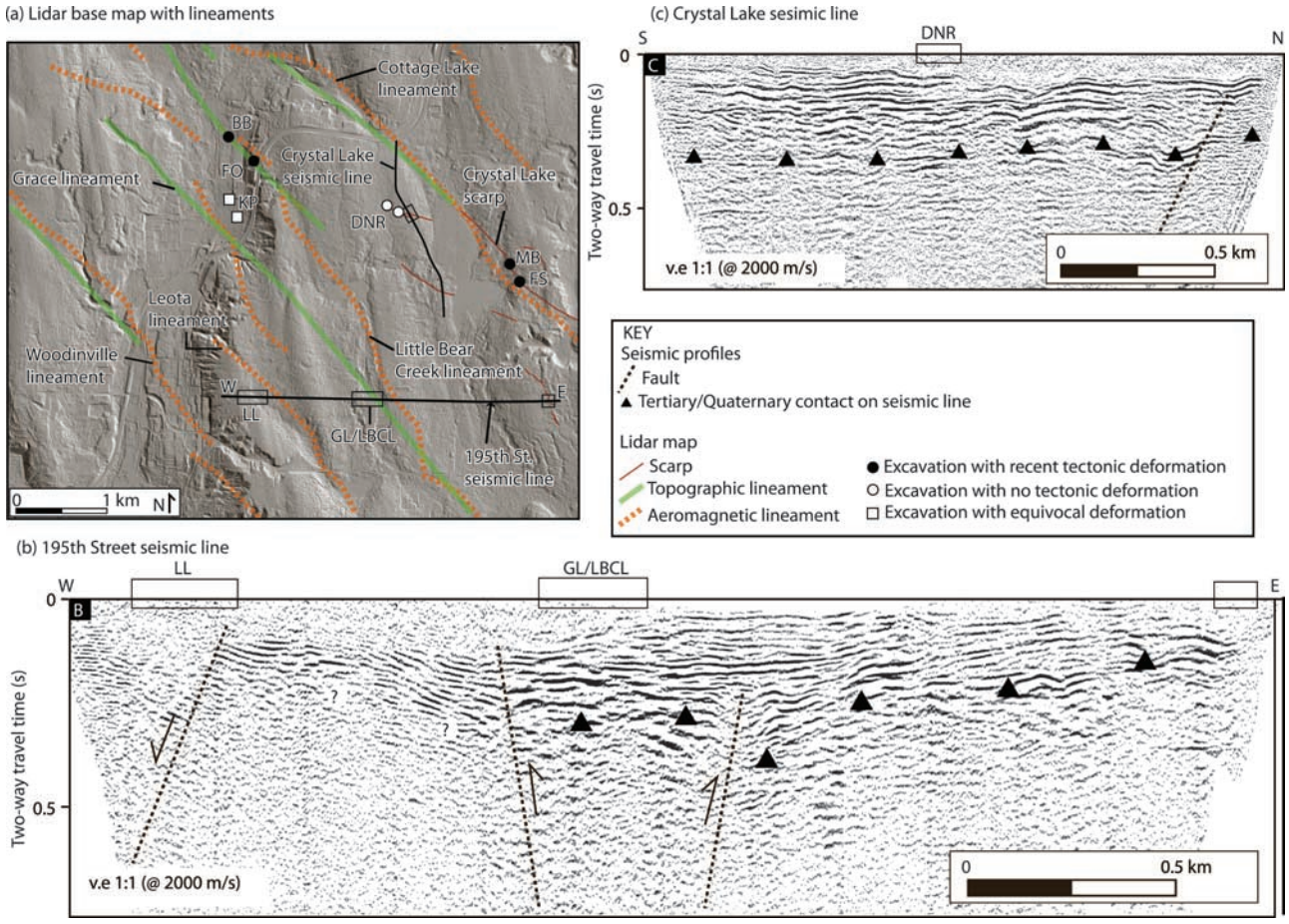

Figure 12. (a) Interpreted bald Earth lidar image showing locations of magnetic lineaments, lidar features, and seismic reflection profiles. (b) Seismic reflection profile along 195th Street showing a zone of deformation where the Grace lineament and the Leota lineament cross the profile. (c) Seismic reflection profile along the west side of Crystal Lake.

push the older laminated claystone up and over the younger massive mudstone, suggesting a reverse sense of motion on this set of faults.

[56] A set of north dipping faults bisected the south dipping fabric in the northern part of the excavation. Offset bedding along the largest of the north dipping faults was not observed so it was not possible to indicate a sense of slip for this set of faults.

[57] A subhorizontal shear fabric cuts across the north dipping and south dipping faults in the French Onion excavation. Microfaults observed in the subhorizontal fabric had both reverse and normal displacements, but were dominated by normal displacement. In general, the sense of net tectonic transport on the microfaults was to the south. South directed tectonic transport is consistent with the subhorizontal fabric resulting from simple shear at the base of a glacier. *Nelson et al.* [2003a, 2003b] observed similar shear fabrics developed in weathered bedrock immediately below till and attributed the shears to movement of glacial ice across the weathered bedrock surface.

4.6. Seismic Reflection Studies: Leota Lake and Grace Lineaments

[58] We acquired two high-resolution seismic reflection profiles from the Woodinville area to afford a better understanding of several faults within the SWIF [*Pape et al.*, 2006]. The first seismic line, named the 195th Street line, was 2.8 km long and was oriented east-west through a residential area adjacent to the paleoseismic excavations described in sections 4.4 and 4.5 (Figure 12a). The second line was ~2 km long and oriented roughly north-south along the western shore of Crystal Lake. The seismic surveys employed a 120-channel seismograph with 5-m source-receiver spacing. The seismic source was a 200 kg trailer-mounted hammer-drop capable of imaging to depths of 1 km. Data processing included elevation and residual statics, band-pass filter, multiple iterations of velocity analysis and dip move out, and poststack Kirchoff migration [*Yilmaz*, 1987].

[59] The most recognizable contact in the seismic sections (noted by the black triangles in Figure 12b) is located in the upper 100–200 m and is characterized by an abrupt change from flat to gently dipping, subparallel reflectors atop discontinuous, wavy reflectors. We interpret this change in seismic character to represent an unconformity separating Tertiary rocks from overlying Quaternary deposits, consistent in depth to nearby boreholes (Figure 5) [*Rau and Johnson*, 1999]. In the 195th Street section, reflections along the eastern portion of the profile dip westward while

reflections along the western portion of the profile dip to the east.

[60] The 195th Street seismic reflection profile crosses, from west to east, the Leota aeromagnetic lineament, the Grace topographic lineament, the Little Bear Creek aeromagnetic lineament, and an unnamed lidar scarp (Figures 12a and 12b). Deformed strata were observed near each of these lineaments. The most prominent deformation occurs near the center of the seismic section (Figure 12b, label GL/LBCL), where the reflectors are laterally truncated near the synclinal axis of a broad fold. We infer that movement on a fault that coincides with the Grace lineament resulted in deformation of both the unconformity and overlying Quaternary deposits. Faulted strata were also observed near the Leota aeromagnetic lineament (Figure 12b, label LL).

[61] The Crystal Lake seismic reflection profile, in contrast to the 195th Street profile, shows relatively undisturbed reflectors along its entire length (Figure 12c). A feature observed on the lidar maps crosses near the middle of the Crystal Lake seismic reflection profile. This feature, labeled DNR on Figures 12a and 12c, was initially interpreted as a possible fault scarp. However, subsequent excavations across this feature did not show any deformation (see trench log in the auxiliary material).

5. Alternatives to Tectonic Deformation

[62] In addition to tectonic deformation, we considered the possibility that other processes, such as mass wasting, soft sediment deformation, and glaciotectonics, are responsible for the linear topography, folding, reverse faults, and liquefaction features observed along the Cottage Lake and Little Bear Creek scarps. The scarp traverses across an area of landslides observed on the lidar maps near the Mountain Beaver excavation (Figures 7 and 8a), and we attribute the low-angle normal fault observed in the excavation to a past landslide. However, the scarp can be traced outside of the area of landslides, indicating that landslides did not create the scarp. No landslides were identified near the other excavations, precluding mass wasting as a cause for the deformation.

[63] Glaciotectonic deformation is not a viable alternative to explain the deformation observed along both scarps. The scarp along the east side of Crystal Lake cuts across a former till plain, an outwash channel, a postglacial landslide, and subtly deforms the surface of a Holocene wetland north of Crystal Lake, suggesting that the scarp formed long after glacial ice left the area (Figure 8). The association of young liquefaction features with reverse faults in the Beef Barley excavation suggests that strong ground shaking accompanied faulting along the Little Bear Creek scarp.

[64] It is temping to interpret the reverse faults observed in the Beef Barley excavation as a manifestation of liquefaction and soft sediment deformation. However, several observations do not fit that interpretation. Published literature shows that at sites where liquefaction did result in small-scale faulting (almost always normal faulting and rarely, reverse faulting), large-scale lateral spreading and intraformational deformation are almost universally observed [e.g., *Keaton and Anderson*, 1995; *Takada and Atwater*, 2004; *Johnson et al.*, 1996]. The liquefaction features at Beef Barley consisted of fluidized sand injected upward under pressure into overlying units. Liquefaction was accompanied by faulting concentrated in an area less than 1 m wide, not by additional large-scale folding and intraformational deformation. The only large-scale folding observed in the excavation occurred thousands of years before liquefaction and may be the result of glaciotectonism.

[65] Several excavations in areas not traversed by linear magnetic anomalies did not show evidence for tectonic deformation (Figure 12). Two excavations were placed across small scarp-like features identified on lidar maps (label DNR, Figure 12a). We found that the surface soils around the excavations were likely disturbed by later land clearing and landfill. Regardless, the excavations in clayey diamict showed horizontal, conformable strata across the possible scarp, indicating that tectonic deformation had not affected the deposits. If folding occurred at this site in the past, it did not exceed 20 cm, the maximum amount of relief observed on any bed in the excavations. (Copies of the field logs are available in the auxiliary material.)

[66] Deformation observed in several excavations at a sewage treatment project that straddles the SWIF was attributed to glaciotectonic deformation [*Keaton and Perry*, 2006]. These excavations (label KP, Figure 12a), sited to guide design of several buildings, are located between the Little Bear Creek lineament and the Grace lineament (referred to as lineament X by *Sherrod et al.* [2005a]). Deformation observed in the excavations included normal and reverse faulting, liquefaction, and folding (Figure 13). Several buttress unconformities were also identified. Although *Keaton and Perry* [2006] attributed all of the observed deformation to movement of glacial ice across the region in the late Pleistocene, our observations collected during a cursory examination of several excavations suggest a more equivocal interpretation for the excavations. Faulting, folding, and liquefaction observed in one excavation appeared to extend to the regraded ground surface but no demonstrably young deposits (recessional outwash deposits or Holocene soils) existed at the site to show that the deformation was constrained to older glacial deposits (Figure 13). Analysis of borehole records near the foundation excavations also suggests the possibility of near surface deformation [*Yeats and St. Peters*, 2006]. Further research along the Grace lineament in areas where postglacial and Holocene deposits exist may clarify the findings of these equivocal excavations.

6. Discussion

[67] Our investigation of the onshore extension of the SWIF followed a three-pronged approach that proved useful in previous Puget Sound fault investigations, aeromagnetic and lidar mapping, followed by targeted trench excavations of scarps [*Blakely et al.*, 2002; *Nelson et al.*, 2003b; *Sherrod et al.*, 2004; *Johnson et al.*, 2004]. We began with regional knowledge of the SWIF and surrounding faults published by others based on sparse bedrock exposures, potential field anomalies, sparse subsurface information, seismic reflection data, and earthquake locations. Our analysis of high-resolution aeromagnetic data revealed subtle magnetic lineaments onshore. These lineaments are spatially aligned with the SWIF as mapped offshore and on Whidbey Island by *Johnson et al.* [1996]. It was not possible to say from

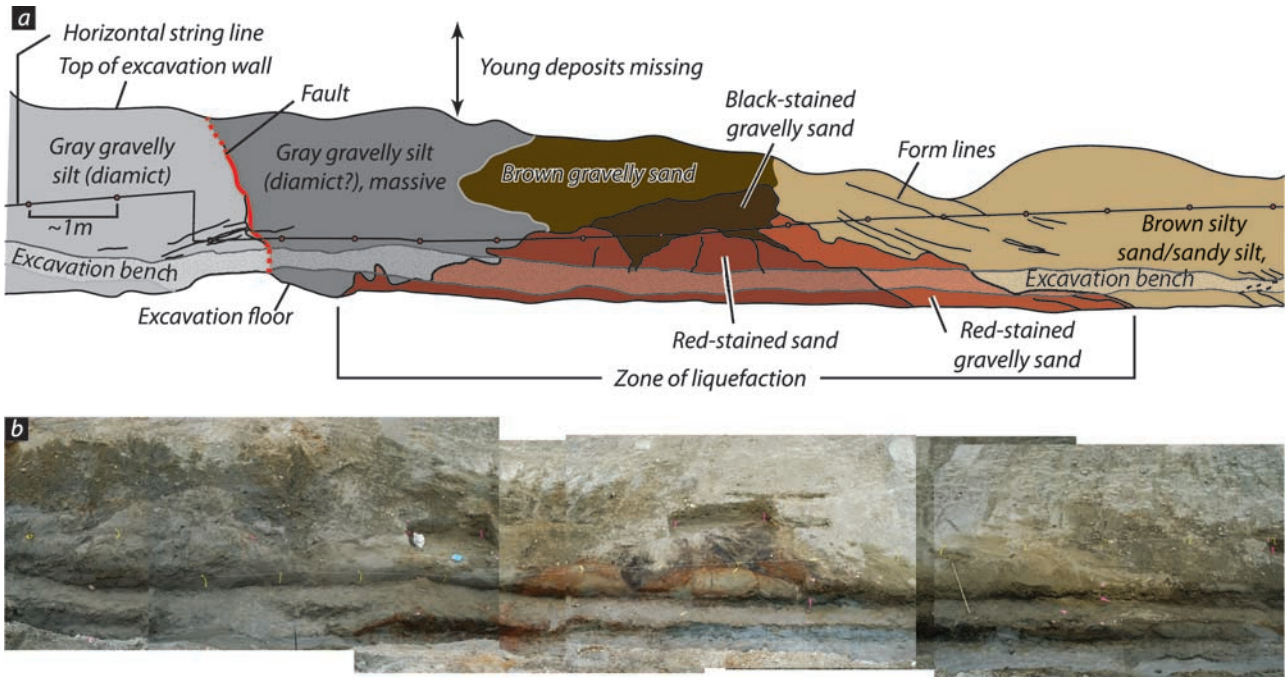

Figure 13. (a) Sketch log drawn from photomosaic (Figure 13b) and observations collected during a visit to a foundation trench excavated by *Keaton and Perry* [2006]. A fault observed in the excavation is indicated by the thick red line. The units filled with red and dark brown are liquefied deposits. Tilted form lines show folding in the sandy silt. (b) Photomosaic of excavation.

magnetic data alone if the magnetic lineaments are caused by faults or some other geologic process. Thus, we turned to lidar mapping, which revealed topographic lineaments and scarps parallel to and sometimes coincident with the aeromagnetic lineaments. This close spatial association strongly suggested that some of the magnetic lineaments have tectonic origins. Finally, trench excavations and seismic reflection transects, guided by lidar and aeromagnetic data, provided a chronology of that tectonic deformation.

6.1. Along-Strike Variation

[68] Figure 14 shows the SWIF in relation to Tertiary and older bedrock and other active structures. As interpreted here, the SWIF extends as a zone of faults a distance of approximately 150 km, from near Victoria, British Columbia, to east of Seattle. Although *Johnson et al.* [1996] showed the northwestern limit of the SWIF terminating in the eastern Strait of Juan de Fuca, *Ramachandran et al.* [2005] more recently suggested on the basis of seismic tomography that the SWIF extends farther to the northwest and merges with the Devils Mountain fault. We have mapped the SWIF southeastward to Woodinville, and we will argue in the following section that the SWIF may extend to east of Seattle and Bellevue.

[69] The SWIF varies in structural style along its 150-km course, generally becoming broader and more complex southeastward. Northwest of Whidbey Island, *Johnson et al.* [1996] mapped the SWIF as two oblique-slip faults, both exhibiting north-side-up, reverse components of displacement. On southern Whidbey Island and in Possession Sound, *Johnson et al.* [1996] showed seismic reflection evidence for three strands of the SWIF, which they interpreted as a flower structure common in oblique-fault settings. Their seismic data showed these strands as discrete faults, with relatively undeformed strata in intervening regions. The SWIF is approximately 7 km wide in Possession Sound.

[70] Aeromagnetic anomalies and lidar scarps indicate that the SWIF broadens to as much as 20 km wide in traversing from Possession Sound to the region between Seattle and Everett. The broad zone onshore consists of numerous overlapping and anastomosing strands, some with lengths up to 20 km. On the basis of available lidar data and our interpretation of aeromagnetic anomalies, these onshore strands are dominated by north-side-up displacement. Magnetic anomaly C (Figure 4), which suggests north-side-down displacement, is a significant exception. Strike-slip displacement is more difficult to detect in lidar and aeromagnetic data but also may have been important.

[71] The change in character of the SWIF along strike may reflect a north-south transition in regional crustal strain [*Miller et al.*, 2001; *McCaffrey et al.*, 2007]. GPS and paleomagnetic data indicate that the central and southern Puget Sound is undergoing north-south contraction caused by the northward translation of the Washington and Oregon Coast Ranges into a relatively stable Canadian buttress [*Wells et al.*, 1998; *Mazzotti et al.*, 2002; *McCaffrey et al.*, 2007]. The southern limit of the Canada buttress is unclear but apparently occurs south of Penticton, British Columbia (Figure 1), where GPS measurements indicate no measurable horizontal translation relative to stable North America [*Wells et al.*, 1998; *McCaffrey et al.*, 2000]. *Miller et al.* [2001] and *McCaffrey et al.* [2007] noted that strain is not uniform throughout the Puget Lowland, but rather rotates from north-south contraction in southern and central Puget Sound to northeast-southwest in the northern Puget Sound.

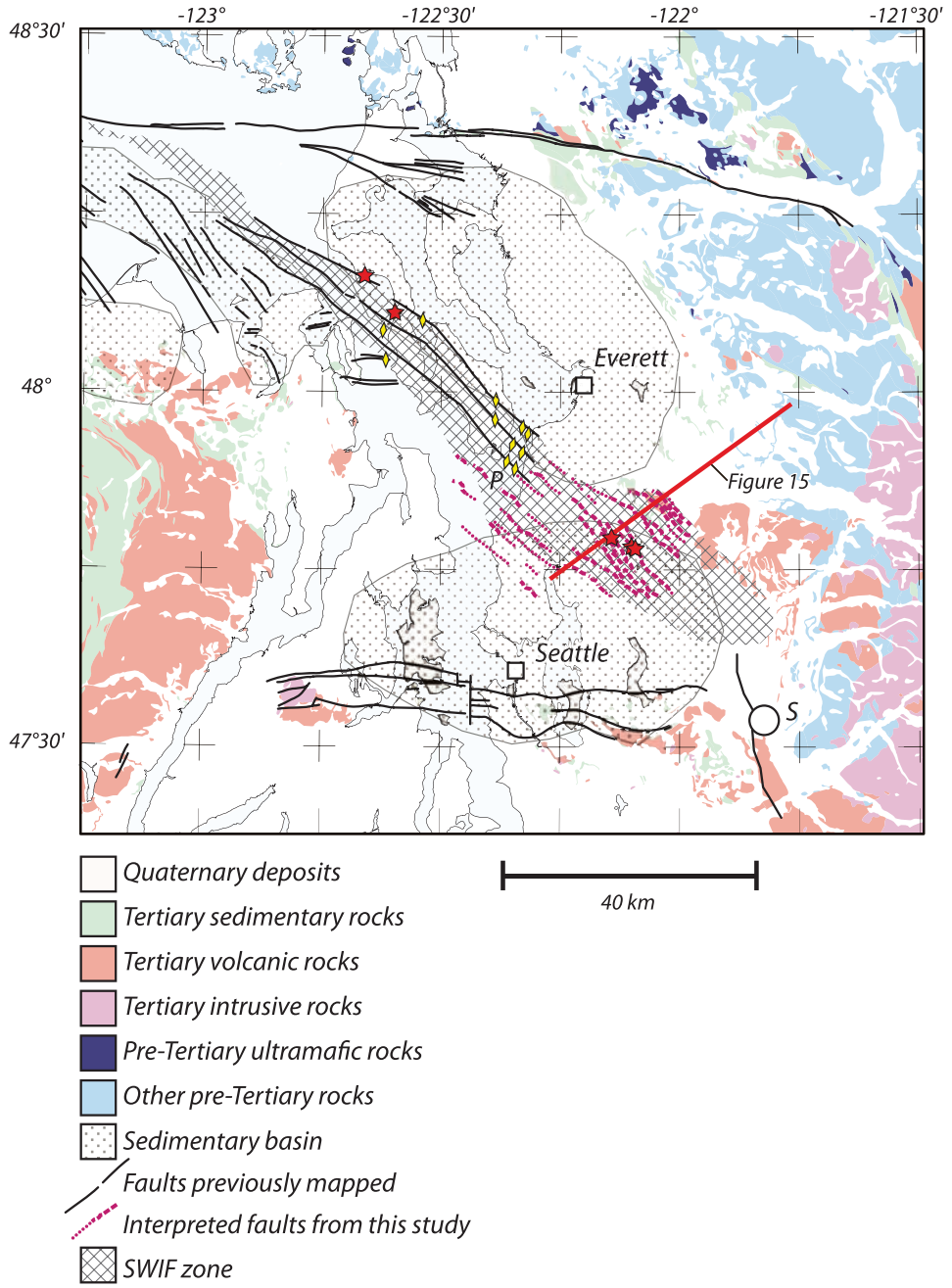

Figure 14. The SWIF in relation to Tertiary and older bedrock and other active structures. Solid black lines are faults from the U.S. Geological Survey Quaternary fault database (http://earthquake.usgs.gov/regional/qfaults). Red dashed and dotted lines are aeromagnetic lineaments discussed in this paper. Yellow diamonds indicate location of Quaternary faults observed by *Johnson et al.* [1996]. Red stars are observations of Holocene deformation discussed in text. Stippled areas are large sedimentary basins manifested in gravity and seismic tomography data. Gray crosshatch pattern indicates the overall width of SWIF deformation. Geologic units generalized from *Dragovich et al.* [2002]. S, Snoqualmie; P, Possession Sound.

In any case, the northwest striking SWIF passes through this deformational transition and may respond at its northwestern end with mostly north-side-up thrust faulting, and at its southeastern end with oblique right-lateral strike-slip behavior. The latter deformational regime may be responsible for the broad zone of faulting between Seattle and Everett.

[72] Seismic data collected across the Grace and Leota Lake aeromagnetic lineaments, interpreted as seismically active from analysis of magnetic and lidar data, provide confirmation of the location of these lineaments and demonstrate that they are tectonically active (Figure 12b) [*Pape et al.*, 2006]. In particular, a seismic reflection line across the Grace lineament shows clear offset of near-surface layers, consistent with tectonic faulting (Figure 12b), although no trenches have been excavated across the Grace lineament as yet. In summary, we conclude on the basis of

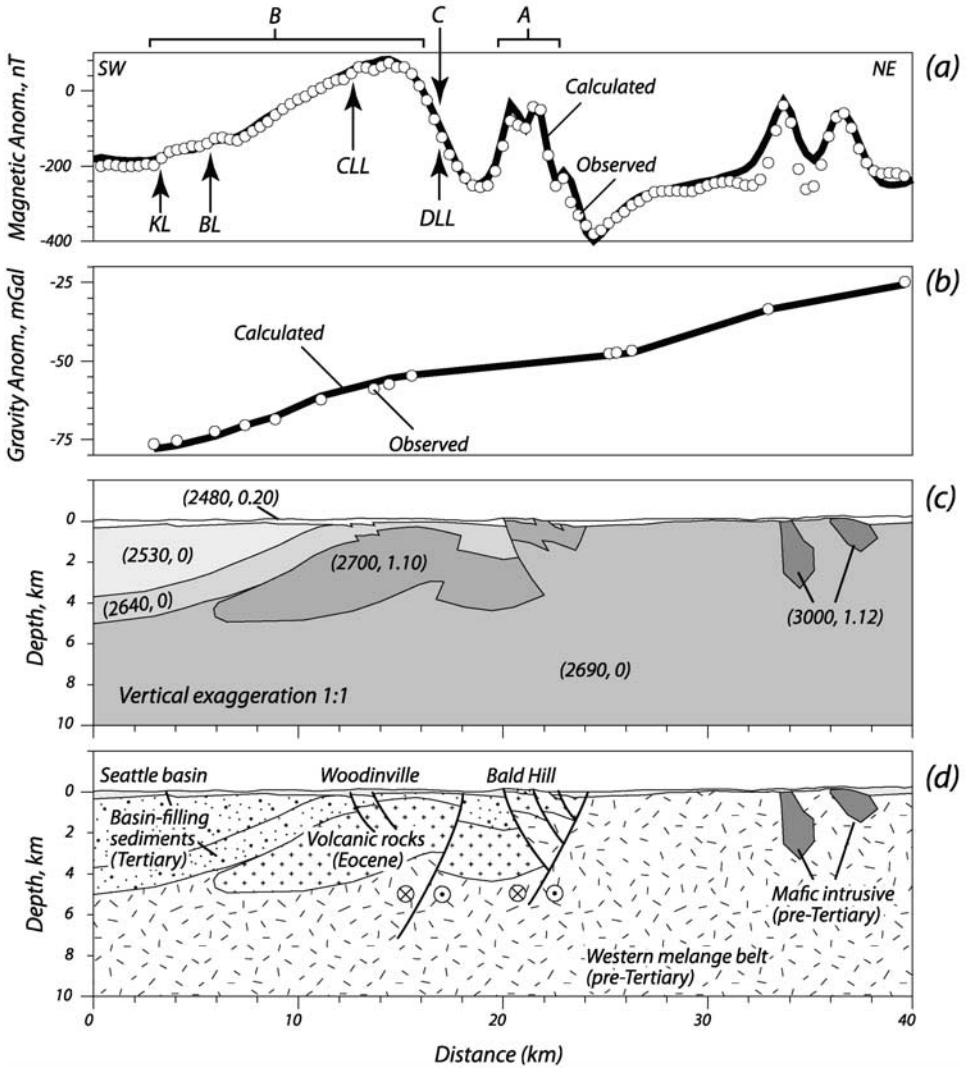

Figure 15. Interpretation of crustal structure across the SWIF in the Woodinville area. Remanent magnetization assumed negligible. Bodies assumed uniform in directions normal to profile. Profile location shown in Figure 2. (a) Observed and calculated magnetic anomalies. Letters refer to aeromagnetic anomalies identified in Figure 4 and discussed in text. (b) Observed and calculated gravity anomalies. (c) Gravity and magnetic model. Numbers in parentheses are density and magnetization, in kg/m^3 and A/m, respectively. (d) Geologic interpretation. Crossed and dotted circles indicate sense of strike-slip displacement.

analysis of magnetic data, lidar images, seismic interpretations, and trench excavations that three aeromagnetic lineaments (Cottage Lake, Little Bear Creek, and Grace) are active strands of the SWIF.

6.2. Regional Crustal Framework of the SWIF

[73] The spatial relationship between the SWIF and the Seattle and Everett basins (Figure 14) may be a clue as to the cause of the broad zone of deformation onshore. From the eastern Strait of Juan de Fuca to Possession Sound, the SWIF follows the southwestern margin of the Everett basin. Southeast of Possession Sound, the SWIF leaves the Everett basin, traverses a basement uplift, and then follows the northeastern margin of the Seattle basin. The Seattle and Everett basins are large crustal structures, 8 to 10 km deep [*Brocher et al.*, 2001; *Johnson et al.*, 1994, 1996], filled with Tertiary and younger sediments, and floored by pre-Tertiary and Tertiary rocks of diverse origins. Perhaps these basins and the intervening uplift influence regional stress patterns, manifested as changes in fault patterns at Possession Sound. Specifically, we hypothesize the broadening of the fault zone can be attributed to along-strike changes in the lithology of shallow bedrock.

[74] Figure 15 shows a possible structural model for the SWIF in the Woodinville area consistent with aeromagnetic, gravity, lidar, and geologic data. It is well known that models based on gravity and magnetic anomalies are nonunique. For any given set of gravity and magnetic data, an infinite variety of mathematically consistent models are possible. Figure 15 shows one such model that is also consistent with independent observations: the abundance of northeast-side-up reverse faults in the Woodinville area, a

pronounced magnetic lineament (Figure 4, label C) with apparent opposite sense of displacement, and exposures of Eocene Mount Persis volcanic rocks at Bald Hill and Devils Butte. We view the SWIF in the Woodinville area as an oblique strike-slip structure, 10 to 20 km in width. The Cottage Lake (Figures 4 and 15, label CLL), Little Bear Creek (Figure 4, label LBCL), and other lidar scarps and subtle magnetic lineaments in the Woodinville area reflect northeast dipping back thrusts within the hanging wall of a larger oblique, southwest dipping reverse fault (Figures 4 and 15, label DLL) that has uplifted volcanic rocks of Mount Persis to near the topographic surface. This reverse fault produces anomaly C (Figures 4 and 15, label C). A second reverse fault, also consistent with aeromagnetic data, is proposed in order to bring Eocene volcanic rocks to the topographic surface at Bald Hill and Devils Butte. It is important to recognize that aeromagnetic anomalies and geologic arguments are our only evidence for the southwest dipping reverse faults at present. Future lidar and geologic investigations may help illuminate these structures. Meanwhile, our intent in presenting Figure 15 is to show that observed lidar scarps and aeromagnetic anomalies in the Woodinville area are consistent with a highly generalized model of oblique-slip deformation.

6.3. Interaction of the SWIF With Other Active Faults

[75] If continued southeastward beyond Woodinville, the SWIF would merge, spatially at least, with the Seattle fault zone at about the location of Snoqualmie (Figure 14, label S) about 35 km east of Seattle. The east-west trending Seattle fault zone is the structural boundary between the Seattle uplift to the south, underlain by Eocene Crescent Formation exposed at the surface, and the Seattle basin to the north, where the same Eocene rocks form the basement surface at ~10 km depth. This extraordinary vertical displacement reflects long-term deformation. *Johnson et al.* [1994] and *Pratt et al.* [1997] interpreted the Seattle fault as a series of south dipping thrust faults, which have moved the Seattle uplift up and over the Seattle basin. *Brocher et al.* [2004] envisioned the Seattle fault to be a north verging triangle zone bounded on the top and bottom by roof and floor thrusts, respectively. In either interpretation, the Seattle fault is well recognized as a significant earthquake hazard to the central Puget Sound [*Bucknam et al.*, 1992; *Nelson et al.*, 2003a, 2003b].

[76] According to *Johnson et al.* [1996], the SWIF and Seattle fault began their evolution in Eocene time as a dextral strike-slip boundary accommodating rifting along the continental margin. At ca. 40 Ma, dextral shear transferred eastward, causing a reorganization of regional fault geometry and giving birth to the SWIF and Seattle fault. *Johnson et al.* [1996] argued that continued offset on the SWIF was linked by concealed faults along the northeastern flank of the Seattle basin to a broad zone of deformation in the eastern Puget Lowland and Cascade foothills. We suggest that this linkage may continue today in the form of the Rattlesnake Mountain fault [*Walsh*, 1984] and other nearby Holocene structures.

[77] West of Snoqualmie, regional north-south contraction is apparently partitioned between thrust fault displacement on the Seattle fault and oblique fault displacement on the SWIF. Assuming that north-south contraction does not terminate at the longitude of Snoqualmie, the Seattle fault and SWIF apparently merge and continue east of Snoqualmie, carrying with it all of the strain shared by the two faults west of Snoqualmie. *Johnson et al.* [1996] suggested that the Seattle fault terminates at the SWIF, and that the SWIF continues southward along a major fault referred to as the Coast Range Boundary Fault. In their view, the Coast Range Boundary Fault and thus all deformation associated with the Seattle and SWIF is confined west of the Cascade Range.

[78] We agree that the Seattle fault truncates against the SWIF but suggest that the SWIF may extend southeastward across the Cascade Range, where it merges with the Olympic-Wallawa lineament (OWL) [*Raisz*, 1945; *Reidel and Campbell*, 1989]. Assuming that total deformation is roughly uniform, the SWIF east of Snoqualmie would accommodate all of the strain shared by the Seattle fault and the SWIF west of Snoqualmie. However, the clockwise rotation west of the OWL predicts that strain rate decreases SE to near zero at a rotation pole in NE Oregon [*McCaffrey et al.*, 2000]. Unfortunately, our high-resolution aeromagnetic survey does not extend far enough eastward to help map the SWIF through the Cascade Range. Future lidar and aeromagnetic surveys may provide evidence to support or refute our conjectures.

6.4. Postglacial Earthquakes on the SWIF

[79] Recurrence of postglacial earthquakes along the SWIF is based on evidence for coastal deformation on Whidbey Island and multiple surface ruptures on the mainland (Figure 16). Coastal stratigraphy of two salt marshes on Whidbey Island show that an earthquake caused more that 1–2 m of north-side-up shoreline warping ~2800–3200 years ago [*Kelsey et al.*, 2004]. To the east on the mainland, excavations across fault scarps indicate prehistoric earthquake activity on at least two strands of the SWIF. These excavations, combined with Whidbey Island coastal deformation [*Johnson et al.*, 1996], suggest that up to four earthquakes struck the SWIF since deglaciation 16,400 years ago (Figure 16).

[80] Recurrence intervals for earthquakes on the SWIF vary widely. The longest recurrence interval is 9200 to 8800 years long and the shortest recurrence interval is 470 years. We determined the longer interval by calculating the difference between the youngest folding event in the Mountain Beaver excavation and the youngest event found in the Beef Barley excavation: the time period between these events is the longest observed (Figure 16). We determined the shortest interval by taking the difference between the limiting minimum age of coastal uplift on Whidbey Island (2870 cal years B.P. [*Kelsey et al.*, 2004]) and the limiting maximum even age observed in the Beef Barley excavation (2730 cal years B.P., Figure 16). The lack of overlapping ages between these two events suggests either a single event or two closely separated events earthquakes occurred on the SWIF between 3200 and 2730 cal years B.P. If we liberally assume two late Holocene events, this yields a minimum recurrence interval of 470 years.

[81] In addition to the events described in Figure 16, one additional earthquake and at least three additional ground shaking events possibly occurred along the SWIF, as evidenced by a possible early Holocene event identified in the Beef Barley excavation (described in section 4.4) and

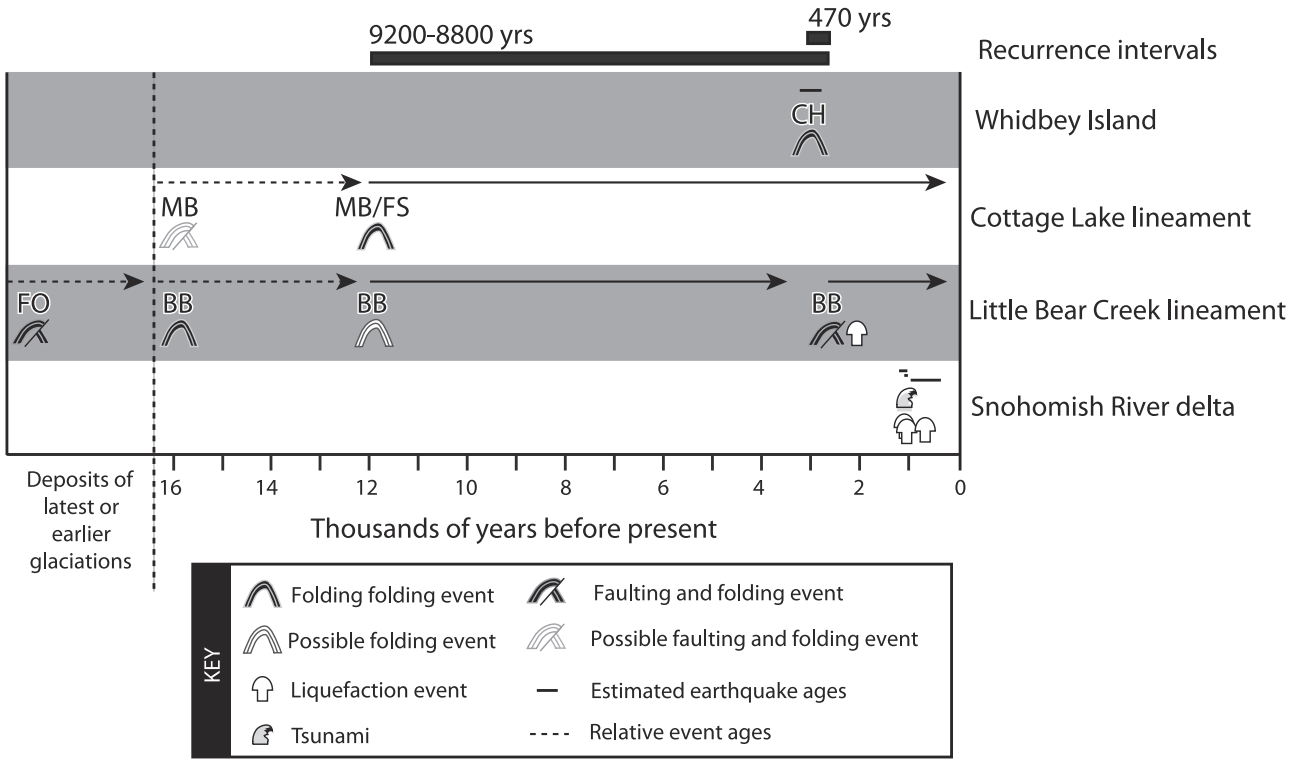

Figure 16. Summary diagram of paleoseismological evidence along the SWIF. Icons indicate the type of event and the lines (or arrows) above each event indicate the estimated limiting ages of the event. BB, Beef Barley; CH, Crockett and Hancock Lakes [*Kelsey et al.*, 2004]; FO, French Onion; FS, Flying Squirrel; MB, Mountain Beaver. Events shown at Snohomish River delta are from *Bourgeois and Johnson* [2001].

deformation observed at the Snohomish River delta [*Bourgeois and Johnson*, 2001]. Including these additional events would imply as many as eight earthquakes on the SWIF during the last 16,400 years. It is important to recognize, however, that these additional liquefaction events may have seismic sources other than the SWIF. The M7 earthquake that occurred on the Seattle fault 1100 years ago [*Bucknam et al.*, 1992] or a local intraslab event may have been responsible for these ground-shaking episodes.

[82] We can make crude estimates of slip during the SWIF earthquakes. Maximum slip, for example, is provided by scarp heights and suggest as much as 4 m of reverse slip, assuming the scarps were formed during a single event. Slip also can be estimated stratigraphically from the excavations and from the coastal marsh study of *Kelsey et al.* [2004]. Coastal marsh stratigraphy suggests that an earthquake about 2800 years ago yielded a minimum vertical offset of 1–2 m [*Kelsey et al.*, 2004], while stratigraphic offsets in the excavations suggest minimum offsets of <1 m and a maximum of 2 m. Using empirical relationships between maximum displacement and magnitude, these offsets correspond to earthquakes between M6.4 and M7.1 [*Wells and Coppersmith*, 1994].

6.5. Earthquake Hazard Implications

[83] Our results have three immediate consequences for earthquake hazard assessments. First, we extend the length of the SWIF from the shoreline of Puget Sound southeastward for at least 30 km to the Woodinville area and speculate that it continues an additional 30 km to a junction with the Seattle fault. Thus, the SWIF extends from Victoria, British Columbia to the vicinity of Snoqualmie, Washington, a total length of about 150 km. It is possible, as suggested in section 6.3, that the fault zone continues even farther to the southeast. Second, paleoseismic studies indicate that the SWIF has generated at least four $M > 6$ to $M \sim 7$ earthquakes during postglacial time. Third, the SWIF becomes structurally more complex southeast of the mainland coast; three strands mapped across Whidbey Island expand to perhaps a dozen strands in the Woodinville area (Figure 4).

7. Conclusions

[84] We applied an analysis of aeromagnetic anomalies, lidar mapping, and paleoseismic investigations to map and characterize the southern Whidbey Island fault (SWIF). The SWIF extends approximately 150 km, from near Victoria, British Columbia, to east of Seattle, where it possibly merges with the Seattle fault 35 km east of Seattle. We infer that strain from the Seattle fault is apparently transferred to a southeastward continuation of the SWIF. Our focus has been the mainland of Washington, where the SWIF passes through heavily populated regions between the cities of Seattle and Everett. Linear magnetic anomalies spatially associated with topographic scarps strongly argue for tectonic origins, and four trench excavations across two of the scarps confirm this conjecture. Along-strike variation in structural style may be caused by north-south variations

in regional stress directions. Paleoseismic studies of the four trenches, when combined with previous work on Whidbey Island marshes, indicate that at least three and possibly as many as eight earthquakes have occurred during the last 16,400 years with magnitudes of M > 6 to M ~ 7.

[85] Our detailed study of the section of the SWIF near Cottage Lake allows us to define three active strands of the fault zone, the Cottage Lake, Little Bear Creek and Grace faults. From these results, we conclude that the distribution of aeromagnetic lineaments in the greater Woodinville area is an indicator of active fault strands. The increased length of the SWIF combined with its unusual width along its southeastern extension will be key issues in upcoming versions of the National Seismic Hazard maps [*Frankel et al.*, 2002].

[86] **Acknowledgments.** Discussions with many of our colleagues helped refine our ideas about the southern Whidbey Island fault. We are particularly grateful to Ray Wells, Tom Brocher, Dave McCormack, Ralph Haugerud, Kathy Troost, and Derek Booth. We also thank Robert Yeats, Robert Simpson, Jan Bednarski, Samual Johnson, and Kelin Wang for comprehensive reviews of our manuscript. Lidar data were graciously provided by the Puget Sound Lidar Consortium and King County.

References

Aspect Consulting (2005), North mitigation area trench boring investigation summary—Brightwater Treatment Plant seismicity investigation, report, Dep. of Nat. Resour. and Parks, Waste Treat. Div., King County, Seattle, Wash.

Atwater, B. F., and A. L. Moore (1992), A tsunami ~1000 yr ago in Puget Sound, Washington, *Science*, *258*, 1614–1617, doi:10.1126/science.258.5088.1614.

Blakely, R. J. (1995), *Potential Theory in Gravity and Magnetic Applications*, 441 pp., Cambridge Univ. Press, Cambridge, U.K.

Blakely, R. J., and R. W. Simpson (1986), Approximating edges of source bodies from magnetic or gravity anomalies, *Geophysics*, *51*, 1494–1498, doi:10.1190/1.1442197.

Blakely, R. J., R. E. Wells, and C. S. Weaver (1999), Puget Sound aeromagnetic maps and data, *U.S. Geol. Surv. Open File Rep.*, *99-514*, 4 pp.

Blakely, R. J., R. E. Wells, C. S. Weaver, and S. Y. Johnson (2002), Location, structure, and seismicity of the Seattle fault zone, Washington: Evidence from aeromagnetic anomalies, geologic mapping, and seismic-reflection data, *Bull. Geol. Soc. Am.*, *114*, 169–177, doi:10.1130/0016-7606(2002)114<0169:LSASOT>2.0.CO;2.

Blakely, R. J., B. L. Sherrod, R. E. Wells, C. S. Weaver, D. H. McCormack, K. G. Troost, and R. A. Haugerud (2004), The Cottage Lake aeromagnetic lineament: a possible onshore extension of the southern Whidbey Island fault, Washington, *U.S. Geol. Surv. Open File Rep.*, *2004-120*, 460 pp.

Booth, D. B., B. F. Cox, K. G. Troost, and S. A. Shimel (2004), Composite geologic map of the Sno-King area, scale 1:24,000, Seattle-Area Geol. Mapp. Proj., Univ. of Wash., Seattle.

Bourgeois, J., and S. Y. Johnson (2001), Geologic evidence of earthquakes at the Snohomish delta, Washington, in the past 1200 yr, *Geol. Soc. Am. Bull.*, *113*, 482–494, doi:10.1130/0016-7606(2001)113<0482:GEOEAT>2.0.CO;2.

Brocher, T. M., T. Parsons, R. J. Blakely, N. I. Christensen, M. A. Fisher, R. E. Wells, and SHIPS Working Group (2001), Upper crustal structure in Puget Lowland, Washington: Results from 1998 Seismic Hazards Investigation in Puget Sound, *J. Geophys. Res.*, *106*, 13,541–13,564, doi:10.1029/2001JB000154.

Brocher, T. M., R. J. Blakely, and R. E. Wells (2004), Interpretation of the Seattle uplift, Washington, as a passive roof duplex, *Bull. Seismol. Soc. Am.*, *94*, 1379–1401, doi:10.1785/012003190.

Brocher, T. M., R. J. Blakely, R. E. Wells, B. L. Sherrod, and K. Ramachandran (2005), The transition between N-S and NE-SW directed crustal shortening in the central and northern Puget Lowland: New thoughts on the southern Whidbey Island Fault, *Eos Trans. AGU*, *86*(52), Fall Meet. Suppl., Abstract S54A-06.

Bucknam, R. C., E. Hemphill-Haley, and E. B. Leopold (1992), Abrupt uplift within the past 1700 years at southern Puget Sound, Washington, *Science*, *258*, 1611–1614, doi:10.1126/science.258.5088.1611.

Dragovich, J. D., R. L. Logan, H. W. Schasse, T. J. Walsh, W. S. Lingley Jr., D. K. Norman, W. J. Gerstel, T. J. Lapen, J. E. Schuster, and K. D. Meyers (2002), Geologic map of Washington-Northwest quadrant, *Geol. Map GM-50*, 72 pp. pamphlet, 3 sheets, scale 1:250,000, Wash. Div. of Geol. and Earth Resour., Olympia.

Frankel, A. D., et al. (2002), Documentation for the 2002 update of the national seismic hazard maps, *U.S. Geol. Surv. Open File Rep.*, *02-420*.

Gower, H. D., J. C. Yount, and R. S. Crosson (1985), Seismotectonic map of the Puget Sound region, Washington, *U.S. Geol. Surv. Misc. Invest. Ser. Map*, *I-1613*, 15 pp., scale 1:250,000.

Johnson, S. Y., C. J. Potter, and J. M. Armentrout (1994), Origin and evolution of the Seattle Fault and Seattle Basin, Washington, *Geology*, *22*, 71–74, doi:10.1130/0091-7613(1994)022<0071:OAEOTS>2.3.CO;2.

Johnson, S. Y., C. J. Potter, J. M. Armentrout, J. J. Miller, C. A. Finn, and C. S. Weaver (1996), The southern Whidbey Island Fault: An active structure in the Puget Lowland, Washington, *Geol. Soc. Am. Bull.*, *108*, 334–354, doi:10.1130/0016-7606(1996)108<0334:TSWIFA>2.3.CO;2.

Johnson, S. Y., et al. (2004), Evidence for late Holocene earthquakes on the Utsalady Point Fault, northern Puget Lowland, Washington, *Bull. Seismol. Soc. Am.*, *94*(6), 2299–2316, doi:10.1785/0120040050.

Karlin, R., and S. E. Abella (1996), A history of Pacific Northwest earthquakes recorded in Holocene sediments from Lake Washington, *J. Geophys. Res.*, *101*(B3), 6137–6150, doi:10.1029/95JB01626.

Keaton, J. R., and L. R. Anderson (1995), Mapping liquefaction hazards in the Wasatch Front region: Opportunities and limitations, in *Environmental and Engineering Geology of the Wasatch Front Region*, edited by W. R. Lund, *Utah Geol. Assoc. Publ.*, *24*, 453–468.

Keaton, J. R., and D. L. Perry (2006), Chemical building seismic trenches, Brightwater wastewater treatment plant site, Snohomish County, Washington, report, 59 pp., 6 appendices, King County Dep. of Nat. Resour. and Parks, Wastewater Treat. Div., Seattle, Wash.

Kelsey, H. M., B. L. Sherrod, S. Y. Johnson, and S. V. Dadisman (2004), Land-level changes from a late Holocene earthquake in the northern Puget Lowland, Washington, *Geology*, *32*, 469–472, doi:10.1130/G20361.1.

Mazzotti, S., H. Dragert, R. D. Hyndman, M. M. Miller, and J. A. Henton (2002), GPS deformation in a region of high crustal seismicity: N. Cascadia forearc, *Earth Planet. Sci. Lett.*, *198*, 41–48, doi:10.1016/S0012-821X(02)00520-4.

McCaffrey, R., M. D. Long, C. Goldfinger, P. C. Zwick, J. L. Nabelek, C. K. Johnson, and C. Smith (2000), Rotation and plate locking at the southern Cascadia subduction zone, *Geophys. Res. Lett.*, *27*(19), 3117–3120, doi:10.1029/2000GL011768.

McCaffrey, R., A. I. Qamar, R. W. King, R. Wells, G. Khazaradze, C. A. Williams, C. W. Stevens, J. J. Vollick, and P. C. Zwick (2007), Fault locking, block rotation and crustal deformation in the Pacific Northwest, *Geophys. J. Int.*, *169*, 1315–1340, doi:10.1111/j.1365-246X.2007.03371.x.

McCormack, D. H. (2003), Subsurface geology of the Brightwater tunnel corridor, western King and Snohomish counties, Washington, *Geol. Soc. Am. Abstr. Programs*, *35*(6), 216.

Miller, M. M., D. J. Johnson, C. M. Rubin, H. Dragert, K. Wang, A. Qamar, and C. Goldfinger (2001), GPS-determination of along-strike variation in Cascadia margin kinematics: Implications for relative plate motion, subduction zone coupling, and permanent deformation, *Tectonics*, *20*, 161–176, doi:10.1029/2000TC001224.

Minard, J. P. (1985), Geologic map of the Maltby quadrangle, Snohomish and King counties, Washington, *U.S. Geol. Surv. Misc. Field Stud.*, *MF-1746*, scale 1:24,000.

Nelson, A. R., S. Y. Johnson, H. M. Kelsey, B. L. Sherrod, R. E. Wells, K. Okumura, L.-A. Bradley, R. Bogar, and S. F. Personius (2003a), Field and laboratory data from an earthquake history study of the Waterman Point fault, Kitsap County, Washington, *U.S. Geol. Surv. Misc. Field Stud. Map*, *MF-2423*.

Nelson, A. R., S. Y. Johnson, H. M. Kelsey, R. E. Wells, B. L. Sherrod, S. K. Pezzopane, L.-A. Bradley, R. D. Koehler III, and R. C. Bucknam (2003b), Late Holocene earthquakes on the Toe Jam Hill fault, Seattle fault zone, Bainbridge Island, Washington, *Geol. Soc. Am. Bull.*, *115*, 1388–1403, doi:10.1130/B25262.1.

Pape, K., L. M. Liberty, and T. Pratt (2006), High resolution seismic reflection imaging of the southern Whidbey Island fault, northwest Washington State, *Eos Trans. AGU*, *87*(52), Fall Meet. Suppl., Abstract S53B-1324.

Peters, L. J. (1949), The direct approach to magnetic interpretation and its practical application, *Geophysics*, *14*, 290–320, doi:10.1190/1.1437537.

Porter, S. C., and T. W. Swanson (1998), Radiocarbon age constraints on rates of advance and retreat of the Puget lobe of the Cordilleran ice sheet during the last glaciation, *Quat. Res.*, *50*, 205–213, doi:10.1006/qres.1998.2004.

Pratt, T. L., S. Johnson, C. Potter, W. Stephenson, and C. Finn (1997), Seismic reflection images beneath Puget Sound, western Washington State: The Puget lowland thrust sheet hypothesis, *J. Geophys. Res.*, *102*, 27,469–27,489, doi:10.1029/97JB01830.

Raisz, E. (1945), The Olympic-Wallowa Lineament, *Am. J. Sci.*, *243-A*, 479–485.

Ramachandran, K., S. E. Dosso, G. D. Spence, R. D. Hyndman, and T. M. Brocher (2005), Forearc structure beneath southwestern British Columbia: A three-dimensional tomographic velocity model, *J. Geophys. Res.*, *110*, B02303, doi:10.1029/2004JB003258.

Ramsey, C. B. (1995), Radiocarbon calibration and analysis of stratigraphy—The OxCal program, *Radiocarbon*, *37*, 425–430.

Rau, W. W., and S. Y. Johnson (1999), Well stratigraphy and correlations, western Washington and northwestern Oregon, *U.S. Geol. Surv. Geol. Invest. Ser.*, *Map I-2621*, 31 pp.

Reidel, S. P., and N. P. Campbell (1989), Structure of the Yakima Fold Belt, central Washington, in *Geologic Guidebook for Washington and Adjacent Areas*, *Inf. Circ.*, vol. 86, edited by N. L. Joseph, et al., pp. 277–304, Wash. Div. of Geol. and Earth Resour., Olympia.

Sherrod, B. L. (2001), Evidence for earthquake-induced subsidence ~1100 yr ago in coastal marshes of southern Puget Sound, Washington, *Geol. Soc. Am. Bull.*, *113*, 1299–1311, doi:10.1130/0016-7606(2001)113<1299:EFEISA>2.0.CO;2.

Sherrod, B. L., T. M. Brocher, C. S. Weaver, R. C. Bucknam, R. J. Blakely, H. M. Kelsey, A. R. Nelson, and R. A. Haugerud (2004), Holocene fault scarps near Tacoma, Washington, *Geology*, *32*, 9–12, doi:10.1130/G19914.1.

Sherrod, B. L., R. J. Blakely, C. S. Weaver, H. M. Kelsey, E. Barnett, and R. Wells (2005a), Holocene fault scarps and shallow magnetic anomalies along the southern Whidbey Island fault zone near Woodinville, Washington, *U.S. Geol. Surv. Open File Rep.*, *2005-1036*.

Sherrod, B. L., E. Barnett, and H. M. Kelsey (2005b), Excavation logs of two trenches across a strand of the southern Whidbey Island Fault Zone near Grace, Washington, *U.S. Geol. Surv. Open File Rep.*, *2005-1013*.

Stuiver, M., et al. (1998), INTCAL98 radiocarbon age calibration, 24,000–0 cal BP, *Radiocarbon*, *40*, 1041–1084.

Tabor, R. W., V. A. Frizzell Jr., D. B. Booth, R. B. Waitt Jr., J. T. Whetten, and R. E. Zartman (1993), Geologic map of the Skykomish River 30-minute by 60-minter quadrangle, Washington, *U.S. Geol. Surv. Misc. Invest. Ser. Map, I-1963*.

Takada, K., and B. F. Atwater (2004), Evidence for Liquefaction Identified in Peeled Slices of Holocene Deposits along the Lower Columbia River, Washington, *Bull. Seismol. Soc. Am.*, *94*, 550–575, doi:10.1785/0120020152.

Walsh, T. J. (1984), Geology and coal resources of central King County, Washington, *Open File Rep. 84-3*, 24 pp., 3 plates, Wash. Div. of Geol. and Earth Resour., Olympia.

Wells, D. L., and K. J. Coppersmith (1994), New empirical relationships among magnitude, rupture length, rupture width, rupture area, and surface displacement, *Seismol. Soc. Am. Bull.*, *84*, 974–1002.

Wells, R. E., and R. W. Simpson (2001), Northward migration of the Cascadia forearc in the northwestern U.S. and implications for subduction deformation, *Earth Planets Space*, *53*, 275–283.

Wells, R. E., C. S. Weaver, and R. J. Blakely (1998), Fore-arc migration in Cascadia and its neotectonic significance, *Geology*, *26*, 759–762, doi:10.1130/0091-7613(1998)026<0759:FAMICA>2.3.CO;2.

Yeats, R. S., and K. St. Peters (2006), Review of borehole logs and reports for the Brightwater regional wastewater treatment plant, Snohomish County, Washington, report, City of Woodinville, Woodinville, Wash.

Yilmaz, O. (1987), *Seismic Data Processing*, 526 pp., Soc. of Explor. Geophys., Tulsa, Okla.

Yount, J. C., and H. D. Gower (1991), Bedrock geologic map of the Seattle 30 × 60 quadrangle, Washington, *U.S. Geol. Surv. Open File Rep.*, *1978*, 91–147.

E. Barnett and H. M. Kelsey, Department of Geology, Humboldt State University, Arcata, CA 95521, USA.

R. J. Blakely, U.S. Geological Survey, 345 Middlefield Road, MS 989, Menlo Park, CA 94025, USA.

L. Liberty and K. Pape, CGISS/Boise State University, 1910 University Drive, Boise, ID 83725, USA.

K. L. Meagher, B. L. Sherrod, and C. S. Weaver, U.S. Geological Survey at Department of Earth and Space Sciences, University of Washington, Seattle, WA 98195, USA.